

 Open access • Posted Content • DOI:10.1101/2021.03.29.437455

Inhibition of PLK1-dependent EBNA2 phosphorylation promotes lymphomagenesis in EBV-infected mice. — Source link

Xiang Zhang, Patrick Schuhmachers, André Mourão, Piero Giansanti ...+13 more authors

Institutions: Helmholtz Zentrum München, University of Zurich, Utrecht University, Technische Universität München ...+1 more institutions

Published on: 30 Mar 2021 - bioRxiv (Cold Spring Harbor Laboratory)

Topics: Transactivation, B cell, PLK1, Kinase and Transcription factor

Related papers:

- [PLK1-dependent phosphorylation restrains EBNA2 activity and lymphomagenesis in EBV-infected mice.](#)
- [EBV epigenetically suppresses the B cell-to-plasma cell differentiation pathway while establishing long-term latency.](#)
- [Proteasomal Inhibition Triggers Viral Oncoprotein Degradation via Autophagy-Lysosomal Pathway](#)
- [Epstein-Barr Virus nuclear antigen 1 \(EBNA1\) confers resistance to apoptosis in EBV-positive B-lymphoma cells through up-regulation of survivin.](#)
- [Contributions of Epstein–Barr Nuclear Antigen 1 \(EBNA1\) to Cell Immortalization and Survival](#)

Share this paper:    

View more about this paper here: <https://typeset.io/papers/inhibition-of-plk1-dependent-ebna2-phosphorylation-promotes-2ccnkgbbdy>

1
2 **Inhibition of PLK1-dependent EBNA2 phosphorylation promotes**
3 **lymphomagenesis in EBV-infected mice.**

4
5
6 Xiang Zhang¹, Patrick Schuhmachers², André Mourão^{3,4}, Piero Giansanti⁵, Anita Murer², Sybille
7 Thumann¹, Cornelia Kuklik-Roos¹, Sophie Beer¹, Stefanie M. Hauck⁶, Wolfgang
8 Hammerschmidt¹, Ralf Küppers⁷, Bernhard Kuster^{5,8}, Monika Raab⁹, Klaus Strebhardt⁹, Michael
9 Sattler^{#3,4}, Christian Münz^{#2}, Bettina Kempkes^{#1}

10
11
12 ¹Research Unit Gene Vectors, Helmholtz Zentrum München, German Research Center for Environmental
13 Health, Feodor-Lynenstr. 21, D-81377 München, Germany

14
15 ²Viral Immunobiology, Institute of Experimental Immunology, University of Zürich, Winterthurerstrasse 190,
16 CH-8057 Zürich, Switzerland

17
18 ³Institute of Structural Biology, Helmholtz Zentrum München, German Research Center for Environmental
19 Health, Ingolstädter Landstrasse 1, D-85764 Neuherberg, Germany

20
21 ⁴Bavarian NMR Center, Department of Chemistry, Technical University of Munich, Lichtenbergstrasse 4,
22 D-85747 Garching, Germany

23
24 ⁵Chair of Proteomics and Bioanalytics, Technical University of Munich, Emil-Erlenmeyer-Forum 5, D-
25 85354, Freising, Germany

26
27 ⁶Research Unit Protein Science and Metabolomics and Proteomics Core Facility, Helmholtz Zentrum
28 München, German Research Center for Environmental Health, Heidemannstrasse. 1, D-80939 München,
29 Germany

30
31 ⁷Institute of Cell Biology (Cancer Research), University Hospital Essen, Virchowstrasse 173, D-45122
32 Essen, Germany

33
34 ⁸Bavarian Center for Biomolecular Mass Spectrometry, Technical University of Munich, Gregor-Mendel-
35 Strasse 4, D-85354, Freising, Germany

36
37 ⁹Department of Gynecology and Obstetrics, Johann Wolfgang Goethe University, Theodor-Stern-Kai 7, D-
38 60590 Frankfurt am Main, Germany

39
40 # Corresponding authors

41

42 **ABSTRACT**

43 While Epstein-Barr virus (EBV) establishes a life-long latent infection in apparently healthy
44 human immunocompetent hosts, immunodeficient individuals are at particular risk to develop
45 lymphoproliferative B cell malignancies caused by EBV. A key EBV protein is the transcription
46 factor EBV nuclear antigen 2 (EBNA2), which initiates B cell proliferation. Here, we combine
47 biochemical, cellular and in vivo experiments demonstrating that the mitotic polo-like kinase 1
48 (PLK1) binds to EBNA2, phosphorylates its transactivation domain and thereby inhibits its
49 biological activity. EBNA2 mutants that impair PLK1 binding or prevent EBNA2 phosphorylation
50 are gain-of-function mutants. They have enhanced transactivation capacities, accelerate the
51 proliferation of infected B cells and promote the development of monoclonal B cell lymphomas
52 in infected mice. Thus, PLK1 coordinates the activity of EBNA2 to attenuate the risk of tumor
53 incidences in favor of the establishment of latency in the infected but healthy host.

54

55 **Keywords:** EBV/ EBNA2/ PLK1/ humanized mice/ B-lymphomagenesis

56

57 **INTRODUCTION**

58 Epstein-Barr virus (EBV) is associated with multiple malignancies including B cell lymphomas
59 and B lymphoproliferative diseases (Farrell, 2019; Longnecker *et al*, 2013; Shannon-Lowe &
60 Rickinson, 2019). More than 90% of the world population are infected with EBV. Based on an
61 intimate virus-host interaction, the virus establishes a latent infection in resting memory B cells
62 (Thorley-Lawson & Gross, 2004). Infected B cells are activated, enter the cell cycle and
63 proliferate and maintain the viral circular genomes in a process that is strictly coordinated with
64 the cell cycle of the host cell. While entering the memory B cell compartment, viral gene
65 expression is gradually silenced to evade host immune surveillance. Reactivation of viral
66 replication and virus production occurs occasionally (Munz, 2019).

67 EBV nuclear antigen 2 (EBNA2) is a key transcription factor that initiates and maintains
68 the expression of viral and cellular target genes which are critical for the growth transformation
69 of B cells by EBV (Kempkes & Ling, 2015; West, 2017). In the nucleus, EBNA2 associates with
70 cellular proteins to execute its function. The B cell-specific transcription factor EBF1 (Friberg *et*
71 *al*, 2015; Glaser *et al*, 2017; Lu *et al*, 2016) and CBF1/RBPJ, the major downstream effector of
72 NOTCH signaling, serve as DNA anchors for EBNA2 (Farrell *et al*, 2004; Henkel *et al*, 1994;
73 Hsieh & Hayward, 1995; Ling & Hayward, 1995). The C-terminal acidic transactivation domain
74 (TAD) of EBNA2 recruits components of the pre-initiation complex and histone acetylases and
75 also contributes to ATP-dependent chromatin remodeling by interacting with hSNF5/Ini (Cohen,

76 1992; Cohen & Kieff, 1991; Cohen *et al*, 1991; Kwiatkowski *et al*, 2004; Tong *et al*, 1995a; Tong
77 *et al*, 1995b; Tong *et al*, 1995c; Wang *et al*, 2000). The TAD of EBNA2 is intrinsically
78 unstructured. In complex with the histone acetylase CBP or the TFIIH subunit Tfb1, a 9-residue
79 amphipathic α -helix within this TAD is formed (Chabot *et al*, 2014). Cellular proteins may control
80 EBNA2 transcriptional activities by protein-protein interactions or modification. The MYND
81 domain of the repressor BS69 can bind as a dimer to the EBNA2 TAD and its flanking regions
82 and attenuates EBNA2 activity as well as transformation efficiency (Harter *et al*, 2016;
83 Ponnusamy *et al*, 2019).

84 In search for additional cellular factors controlling EBNA2 function, we have performed a
85 label-free mass spectrometry-based quantification of cellular proteins in EBNA2 immuno-
86 precipitates and found polo-like kinase 1 (PLK1). PLK1 is a serine/threonine-protein kinase that
87 controls G2/M transition and progress through mitosis and cytokinesis in a tightly controlled
88 order to secure genomic stability of the dividing cell. Through phosphorylation of specific
89 substrates, PLK1 promotes activation of the mitotic driver Cyclin B1/CDK1 in the late G2-phase,
90 triggering prophase onset (Gheghiani *et al*, 2017; Nakajima *et al*, 2003; Watanabe *et al*, 2005).
91 PLK1 recognizes its substrates by a conserved C-terminal polo-box domain (PBD). Frequently,
92 PBD binds to pre-phosphorylated epitopes generated by the mitotic CDK1 kinase or other
93 proline-directed kinases like MAPK (Elia *et al*, 2003a; Elia *et al*, 2003b; Lowery *et al*, 2005). This
94 process is referred to as non-self-priming (Barr *et al*, 2004; Lee *et al*, 2014). Since primary
95 tumors from various tissues express elevated levels of PLK1 and this high-level expression
96 frequently correlates with a poor prognosis (Wolf *et al*, 1997), PLK1 is a potential oncotarget for
97 molecular cancer therapy and a prognostic marker (Rodel *et al*, 2020; Rosenblum *et al*, 2020;
98 Yuan *et al*, 1997). Preclinical and clinical studies currently test potential clinical indications for
99 small molecule or siRNA-based PLK1 inhibitors (Liu *et al*, 2017). However, there is now
100 increasing evidence that PLK1 can also act as a tumor suppressor when expressed in the
101 context of specific tumor types. Thus there is a strong need to define the exact molecular
102 features of tumors that should be treated with PLK1 inhibitors (de Carcer, 2019).

103 Here, we show that PLK1 directly binds to EBNA2. EBNA2/PLK1 complex formation is
104 strongly enforced by EBNA2 residue S379 phosphorylation catalyzed by the mitotic Cyclin
105 B/CDK1 complex. PLK1 phosphorylates the C-terminal transactivation domain of EBNA2 and
106 attenuates its activity. EBNA2 mutants that lack either the main PLK1 docking site or the two
107 phosphorylation sites are gain-of-function mutants that promote lymphoma incidence in EBV-
108 infected humanized mice. This indicates that PLK1 acts as a tumor suppressor in EBV-driven
109 carcinogenesis.

110

111

112 RESULTS

113 *Cyclin B/CDK1 primes EBNA2 residue S379 for Polo-like kinase 1 (PLK1) binding*

114 To identify potential EBNA2 interacting cellular proteins, we transfected EBV-negative DG75 B
115 cells with HA-tagged EBNA2 expression constructs or the corresponding HA-expression vector
116 and performed immunoprecipitations with HA-specific antibodies. Tryptic peptides of these
117 immunoprecipitates were analyzed and quantified by label-free mass spectrometry. Polo-like
118 kinase 1 (PLK1) was one of 19 proteins that were significantly enriched in EBNA2 co-
119 immunoprecipitates (Table EV1). As expected, the EBNA2 DNA anchor protein CBF1/RBPJ
120 was one of these proteins, demonstrating that the experimental approach was valid. Importantly,
121 PLK1 and EBNA2 specifically co-immunoprecipitated from whole cell extracts of EBV-infected B
122 cells in which both proteins are expressed at endogenous physiological levels (Fig. 1).

123 To identify PLK1 docking sites within EBNA2, EBNA2 deletion fragments were
124 generated and tested for binding to PLK1 by transfection and co-immunoprecipitation (Fig. 1A,
125 B, C). The smallest EBNA2 fragment that efficiently bound PLK1 mapped to region 342-474.
126 Sub-fragments of either 327-487 or 342-474 showed some residual binding but none of these
127 regions conferred binding efficiencies similar to the precursor.

128 PLK1 frequently binds to phosphorylated substrates that are primed by cellular kinases
129 like Cyclin B/CDK1. These substrates share a consensus motif [Pro/Phe]-[Φ/Pro]-[Φ]-
130 [Thr/Gln/His/Met]-Ser-[pThr/pSer]-[Pro/X] (Φ represents hydrophobic and X represents any
131 residue) specific for binding to the Polo-box binding domain (PBD) of PLK1 (Elia *et al.*, 2003a).
132 Crystal structures of the PLK1 PBD in complex with peptides demonstrate how the positively
133 charged groove of PBD docks onto negatively charged phosphopeptides of diverse substrates.
134 EBNA2 exhibits three potential Cyclin B/CDK1 phosphorylation/ PBD docking sites located at
135 residue T267, S379 and S470 (Fig. D). Mutants involving the respective residues were tested
136 for PLK1 binding by transfection and co-precipitation. The mutation TSS377VAA impaired PLK1
137 binding dramatically while all other EBNA2 mutations did not affect PLK1 binding (Fig. 1E). To
138 specify the contribution of EBNA2 residue S379 phosphorylation, a heptapeptide (PNTSSPS)
139 and phospho-heptapeptide (PNTSpSPS) were tested for PBD (PLK1 residue 345-603) binding
140 by isothermal titration calorimetry (ITC). The phosphorylated peptide bound PBD in a molar ratio
141 of 1:1 whereas no interaction was detected using the unmodified peptide. The PNTSpSPS/ PBD
142 interaction is micromolar with a dissociation constant of $K_D = 8.19 \mu\text{M}$ (Fig. 1F). GST EBNA2
143 342-422 expressed and purified from bacterial extracts did hardly pull-down any PLK1 from

144 cellular extracts. Phosphorylation of the EBNA2 protein produced in bacteria by Cyclin B/ CDK1,
145 an enzyme not present in bacteria, strongly enhanced PLK1 binding. EBNA2 (342-422) S379A
146 mutant did not bind PLK1 and phosphorylation by Cyclin B/CDK1 could not reconstitute binding
147 (Fig. 1G). Also, as shown by transfection, EBNA2 S379A binding to PLK1 was severely
148 impaired (Fig. 1H). We conclude that EBNA2 residue S379 is a PLK1 docking site primed by
149 Cyclin B/CDK1 phosphorylation.

150
151

152 *The C-terminus of EBNA2 is the substrate of PLK1*

153 In order to test if EBNA2 is phosphorylated by PLK1, EBNA2/PLK1 complexes were co-
154 precipitated from cellular extracts of DG75 cells induced with doxycycline to express HA-EBNA2
155 (DG75^{Dox} HA-EBNA2) (Fig. 3A). The precipitates were submitted to kinase assays either in the
156 presence or absence of exogenous recombinant PLK1. Phosphorylation of EBNA2 was readily
157 detected in the co-precipitates and was enhanced by the addition of exogenous recombinant
158 PLK1 to the co-precipitates (Fig. 3B). EBNA2 phosphorylation was prevented upon addition of
159 Volasertib, a PLK1 specific inhibitor, to the co-precipitates of EBNA2 and endogenous PLK1
160 (Fig. 3C), corroborating the evidence that the endogenous PLK1 trapped in the co-precipitate is
161 the active kinase.

162 To identify the amino acid residues that are phosphorylated by PLK1, bacterially
163 expressed EBNA2 was phosphorylated by active recombinant PLK1 or left untreated. The
164 EBNA2 protein was digested by trypsin and endoproteinase Glu-C (V8 Protease) in parallel.
165 Tryptic or V8 Protease derived peptides and phospho-peptides were identified by mass
166 spectrometry (MS). Since neither tryptic nor V8 derived peptides covered the C-terminus of
167 EBNA2 sufficiently, a subfragment (453-474) of EBNA2 flanked by arginine residues and
168 expressed as a GST fusion protein was used for further tryptic digest and phosphopeptide
169 mapping (Fig. EV1). Initially, 11 potential phosphorylation sites were found. Of these, 5
170 phosphorylation sites (S184, 258, 457, 479 and T465) were confidently localized (Fig. EV2) and
171 6 additional sites (T175, 178, 263, 267, 464 and S266) were ambiguously mapped. To test, if
172 the 5 confident phosphorylation sites identified in vitro are relevant also in cells, EBNA2 mutants
173 with a singular or combined mutations were generated and expressed in DG75 B cells.
174 Immunoprecipitations and subsequent kinase assays based on endogenous PLK1 trapped in
175 the precipitates were performed (Fig. 3D). None of the mutations severely impaired PLK1
176 binding but Volasertib prevented phosphorylation of all EBNA2 proteins. In the absence of
177 Volasertib, phosphorylation of S184A, S258A and S479A was not reduced. Phosphorylation of

178 the EBNA2 mutants S457A and T465V was impaired, and the combination of both mutations
179 (S457A/T465V) abolished phosphorylation (Fig. 3E). To corroborate this finding GST EBNA2
180 246-487 either in wild-type or as S457A/T465V mutant was submitted to kinase assays using
181 recombinant PLK1 in vitro. This experiment resulted in efficient phosphorylation of wild-type but
182 not mutant EBNA2 S457A/T465V (Fig. 3F). We conclude that the PLK1 docking and the PLK1
183 phosphorylation site are two independent EBNA2 modules that can be dissected and analyzed
184 by specific mutations (Fig. 3G).

185 To test the phosphorylation mutants for their biological activity, we used a luciferase
186 reporter construct driven by an EBNA2 responsive artificial promoter that harbors a
187 multimerized CBF1 binding site to recruit EBNA2 (Minoguchi *et al.*, 1997). All mutants that
188 carried either the S457A, the T465V mutation or both mutations showed enhanced
189 transactivation potential, suggesting that PLK1 might negatively regulate EBNA2 activity (Fig.
190 2H). Since the C-TAD of EBNA2 is known to bind the histone acetylase and co-activator p300
191 (Chabot *et al.*, 2014), p300 binding to EBNA2 phosphorylation mutants was tested by GST-
192 pulldown experiments. While p300 binding of the single EBNA2 phosphorylation mutants was
193 strongly enhanced by approximately 2-3-fold, binding by the double mutant S457A/T465V was
194 increased even 8-9-fold. Thus, enhanced p300 binding of EBNA2 phosphorylation mutants
195 correlates well with improved transactivation activity. This finding suggests that PLK1
196 phosphorylation hinders p300 recruitment to EBNA2, thereby inhibiting EBNA2 transactivation
197 (Fig. 3I).

198 To directly test if PLK1 inhibits EBNA2 functions, PLK1 and EBNA2 were co-expressed
199 and luciferase reporter assays were performed. EBNA2 wt activity was significantly reduced by
200 co-expression of PLK1 but not affected by the kinase dead K82M PLK1 mutant. The activity of
201 the docking site mutant S379A was weakly impaired by co-expression of PLK1 suggesting that
202 residual binding activity, as demonstrate in Fig. 2H, might still recruit PLK1 activity. Importantly,
203 the transactivation capacity of the phosphorylation mutant S457A/T465V was not affected by
204 PLK1 co-expression. Since the kinase dead PLK1 mutant did not impair the transactivation
205 capacity of any EBNA2 protein, we conclude that PLK1 binding is necessary but not sufficient to
206 inhibit EBNA2 and the phosphorylation of EBNA2 by PLK1 is required to inhibit EBNA2.

207 In summary, PLK1 phosphorylates S457 and T465 within the TAD of EBNA2 to
208 attenuate its activity and to impair p300 binding. PLK1 uses S379A as a phosphorylation-
209 dependent docking site that can be primed by Cyclin B/CDK1.

210

211

212 *EBV strains expressing EBNA2 mutants deficient for PLK1 docking or phosphorylation are gain-*
213 *of-function mutants in B cell immortalization assays.*

214 To test EBNA2 mutants defective for PLK1 binding or phosphorylation by PLK1 for their B cell
215 immortalization potential, three new viral mutants based on the viral backbone of the
216 recombinant EBV strain p6008 (Mrozek-Gorska *et al*, 2019; Pich *et al*, 2019) were generated.
217 Carboxyl-terminally HA-tagged EBNA2 (EBV wt), HA-tagged EBNA2 S379A (EBV S379A), and
218 HA-tagged EBNA2 S457A/T468V (EBVS457A/T465V) were inserted into the backbone of the
219 recombinant EBV strain p6008 by homologous recombination using a two-step positive-negative
220 selection protocol, also called recombineering (Wang *et al*, 2009). The integrity of the viral
221 genomes was controlled by restriction digest and sequencing (Fig. EV3). Infectious viruses were
222 produced in HEK293 cells. Primary B cells from three unrelated donors were infected. During
223 the first 6 days post-infection, the proliferation rates of EBV wt, EBV S457A/T465V or EBV
224 S379A infected B cells were determined. The phosphorylation mutant S457A/T465V proliferated
225 the fastest, followed by S379A and wt infected cells (Fig.5A and Fig. EV3C, D). Long-term
226 cultures could be established and the proliferation of these lymphoblastoid cell lines (LCLs) was
227 characterized by counting the cells daily (Fig. 5B). The proliferation rates of both long-term
228 cultures infected with mutant viruses were higher than EBV wt infected cells. EBNA2 expression
229 levels in these long-term cultures were similar for wt and S379A but less pronounced for the
230 S457A/T465V mutant. LMP1 expression varied between the cell lines obtained from different
231 donors but was consistently elevated in EBV S457A/T465V infected cell lines compared to
232 S379A and EBV wt infected B cells. MYC expression was seen in all infected cultures and MYC
233 levels were not affected by individual virus variants (Fig. 5C). In summary, both mutants were
234 gain-of-function mutants with respect to proliferative capacities of the infected cell cultures and
235 LMP1 activation. In comparison, these features were more pronounced in EBV S457A/T465V
236 than in S379A infected B cells.

237

238

239 *Enhanced frequencies of B cell lymphomas in humanized mice infected with EBV S379A or*
240 *EBV S457A/T465V*

241 Since EBV does not infect murine B cells, tumor development and immune control were studied
242 in humanized mice. Immunodeficient NSG (NOD scid $\gamma_c^{-/-}$) mice can be engrafted with CD34⁺
243 human hematopoietic progenitor cells to develop human immune system components that can
244 be readily infected with human lymphotropic pathogens, including EBV. These chimeric
245 humanized mice were used previously to study EBV-induced tumor formation after EBV

246 infection and anti-viral immune mechanisms against EBV in vivo (Strowig *et al*, 2009b). Hence,
247 we infected three cohorts (designated experiment 1, 2 and 3) of humanized mice
248 intraperitoneally with 10^5 Green Raji Units (GRU) of EBV and analyzed viral blood loads, CD8⁺
249 and CD4⁺ T cell composition as well as activation in their blood in weekly intervals. Five weeks
250 post-infection, all EBV-positive mice were sacrificed to analyze tumor development (Fig. 6A). In
251 two out of three independent experiments, infection with EBV S457A/T465V caused increased
252 mortality rates compared to EBV wt or S379A infected animals (66% survival in the second and
253 20% in the third experiment; Fig. 6B). In addition, mice that were infected with either of the two
254 EBV mutants presented with higher incidence of tumor development in spleen, peritoneal cavity
255 or lymph nodes (23% for WT, 36% for S379A, and 44% for S457A/T465V; Fig. 6C). Viral loads
256 in the spleen of mice infected with mutants were slightly elevated 5 weeks post-infection when
257 mice were sacrificed (Fig. 6D). In blood, viral loads of EBV wt and EBV S379A infected mice
258 gradually increased until week 3 and remained at similar levels until the end of the experiment.
259 In contrast, viral loads in mice within the EBV S457A/T465V mutant group reached higher levels
260 already two weeks after infection and started to decrease at 4 weeks post-infection (Fig. 6E).

261 Extensive CD8⁺ T cell expansion and activation in blood is a common trait marking EBV
262 infection in humanized mice. It usually follows, with a delay of about a week, rising viral loads
263 (Chatterjee *et al.*, 2019; Strowig *et al.*, 2009) and correlates with these (Caduff *et al*, 2020;
264 Zdimerova *et al*, 2020). As CD8⁺ T cells expand more strongly than CD4⁺ T cells upon EBV
265 infection, a rising CD8⁺ to CD4⁺ T cell ratio indicates the extensive proliferation of CD8⁺ T cells.

266 Three weeks post-infection the mean CD8⁺/CD4⁺ T cell ratios in mice infected with EBV
267 S457A/T465V (0.99) were significantly higher than in EBV wt (0.37) infected mice (Fig. 6F),
268 while CD8⁺/CD4⁺ T cell ratios of EBV wt infected animals increased later, at 4 weeks post-
269 infection (Fig. 6F).

270 CD8 and CD4 T cell populations infected with mutant virus started to expand already 2
271 weeks post-infection (Fig. EV4 A, B). Also, the relative fraction of CD8⁺ T cells expressing the
272 activation marker HLA-DR increased from week 2 post-infection, thus earlier than the control
273 EBV wt infected group (Fig. EV4 C, D). A similar trend could be observed for mice infected with
274 the EBNA2 S379A mutant. Interestingly, the EBV S457A/T465V mutant more strongly induced
275 the activation of CD4⁺ T cells in the blood of mice within 5 weeks of infection compared to the
276 EBV wt infected group (Fig. EV4 D). In contrast to blood, the fractions of CD8⁺ and CD4⁺ T cells
277 in the spleen of infected animals did not differ between the groups (Fig. EV4 E) but a higher
278 fraction of CD8⁺ and a significantly increased fraction of CD4⁺ T cells were HLA-DR-positive and
279 thus activated in EBV S457A/T465V infected animals (Fig. EV4 F, G). The development of

280 memory T cells, i.e. effector memory (Tem), central memory (Tcm) or terminally differentiated
281 subsets that re-express CD45RA (Temra), however, was not influenced by EBNA2 mutations
282 (Fig. EV4 H, I). In summary, EBV S379A and EBV S457A/T465V infections developed more
283 rapidly in humanized mice, resulting in earlier immune responses, increased lymphomagenesis
284 and more frequent demise of the mice.

285
286

287 *Tumors of EBV S379A or EBV S457A/T465V infected mice frequently present as monoclonal B*
288 *cell lymphomas.*

289 The diversity of immunoglobulin gene rearrangements and sequences can be used to define the
290 clonal composition of a given B cell population (Kuppers *et al*, 1993; Rajewsky, 1996). In
291 experiment 2, 1 out of 5 EBV wt, 2 out of 4 EBV S379A and 2 out of 4 EBV S457A/T465V
292 infected mice developed tumors. The clonality of macroscopically visible tumors detected in
293 experiment 2 was assessed by PCR of rearranged IgH V genes, using subgroup specific IgH V
294 primers together with an IgH J primer mix in separate reactions, followed by Sanger sequencing
295 of amplicates obtained (Table 1). Polyclonal B cell expansions were found in the splenic
296 tumors of EBV wt (#13) and in one splenic tumor of EBV S379A (#23). In all of the four analyzed
297 tumor bearing mice infected with mutant EBV, monoclonal B cell populations were identified,
298 sometimes on a background of remaining polyclonal B cells. In mouse #23, the spleen harbored
299 a polyclonal B cell population, while the peritoneum showed a monoclonal B cell expansion.
300 This analysis validates that the tumors developing in EBNA2 mutant mice are indeed
301 monoclonal, and hence bona fide malignant B cell lymphomas. In all five monoclonal
302 lymphomas, productive in-frame IgH V genes were obtained. Three of the samples showed
303 additional out-of-frame rearrangements, which likely represent the second IgH alleles of the
304 monoclonal lymphomas defined by the in-frame rearrangements. Since humanized NOD scid γ_c^-
305 $^-$ mice in the experimental setup of our study cannot generate germinal centers we did not
306 expect somatic hypermutation to occur. Indeed, somatic mutations were not observed in any
307 specimen.

308
309

310 **DISCUSSION**

311 *EBNA2 mutations, which impair PLK1 binding or prevent phosphorylation by PLK1, accelerate*
312 *cellular proliferation and tumor formation.*

313 Our study demonstrates that PLK1 directly binds to the phosphorylated EBNA2 residue S379
314 and phosphorylates S457 and T465 located in the transactivation domain of EBNA2.
315 S457A/T465V missense mutants can still bind to PLK1 but are not phosphorylated. The EBNA2
316 docking site S379A and EBNA2 S457A/T465V phosphorylation mutants, both show enhanced
317 transactivation capacities with S457A/T465V being stronger than S379A. This enhanced
318 potential might be caused in part by the elevated levels of histone acetylase and co-activator
319 p300 that binds to the S457A/T465V mutant. Kinase active but not kinase dead PLK1 (K82M)
320 inhibited EBNA2 wild-type activity and, to a minor extent, the S379A docking site mutant. Since
321 the phosphorylation mutant EBNA2 S457A/T465V was not inhibited by PLK1 co-expression we
322 conclude that EBNA2 phosphorylation, rather than sole PLK1 binding, inhibits the
323 transactivation potential. The residual inhibition of EBNA2 S379A might be caused by PLK1
324 since this mutant retains some PLK1 binding activity and thus can be phosphorylated.

325 Both EBV mutants, which expressed EBNA2 S379A or S457A/T465T were fully
326 immortalization competent and initiated long-term proliferating B cell cultures with accelerated
327 cell division rates and elevated induction of the EBNA2 target gene LMP1. The impact of both
328 mutations was further studied in humanized mice susceptible to EBV infection. Blood samples
329 of infected mice were analyzed weekly for viral loads and immune responses of CD4⁺ and CD8⁺
330 T cell populations. Elevated viral loads and CD4⁺ and CD8⁺ T cell activation in the blood of EBV
331 S457A/T465V of infected mice preceded CD8⁺ T cell expansion. On the day of sacrifice, splenic
332 EBV loads were slightly elevated in both EBNA2 mutants compared to EBV wt infected animals.
333 Based on earlier publications, increasing viral loads were expected to precede expansion and
334 activation of EBV-specific CD8⁺ T cells since antigen abundance stimulates CD8⁺ T cell
335 responses (Shultz *et al*, 2010; Strowig *et al*, 2009a). Irrespective of the early adaptive immune
336 response to infection, more EBV mutant infected mice developed lymphomas when compared
337 to EBV wt infections. The accelerated proliferation rates that we observed in cell culture might
338 contribute to tumor size in mice. The enhanced transcriptional activities of the EBNA2 mutants
339 induce higher LMP1 levels, which is a critical viral oncogene in B cell transformation and thus
340 also might promote tumor formation in vivo. In addition, both EBNA2 mutants might also induce
341 distinct viral and cellular RNAs, which promote tumor progression but still are to be identified.

342 Importantly, tumors detected in mice infected with mutant virus were predominantly
343 monoclonal, and could be detected in the spleen as well as in the peritoneum and in lymph

344 nodes. The elevated viral loads seen in mice infected with mutant EBV might increase tumor
345 incidence by amplifying the number of infected B cells in these animals and thereby might
346 initiate the lymphoproliferative disease at multiple sites but they do not explain disease
347 progression to monoclonal B cell lymphomas. It will be interesting to study if lymphomas in
348 lymph nodes or peritoneum are metastatic descendants of splenic tumors. The genetic or
349 epigenetic processes driving the clonal evolution of single cells and giving rise to monoclonal
350 tumors still need to be explored.

351

352

353 *PLK1 controls the growth transformation potential of EBNA2 to establish tumor free survival of*
354 *latently infected hosts.*

355 Our study suggests that EBNA2 activity needs to be controlled by PLK1 in order to reduce the
356 risk of tumor formation while latency is established in the infected animals. Since PLK1 activity
357 peaks in mitosis, PLK1 might control EBNA2 activities preferentially during this time window.
358 Unfortunately, since during mitosis the global cellular transcription of the condensed
359 chromosomes and the viral episome is silenced, EBNA2 activity cannot be reliably tested in
360 mitotic cells. There appears to be a strict biological necessity to dynamically control EBNA2
361 activity by multiple viral and cellular factors. Transient transfections and reporter gene studies
362 have suggested that Cyclin B/ CDK1 or the viral lytic kinase BGLF4 can control EBNA2 activity,
363 but these studies have not linked their findings to PLK1 activity (Yue *et al*, 2004; Yue *et al*,
364 2005; Yue *et al*, 2006).

365 PLK1 is a key control element of multiple cell cycle stages including G2/M transition, M-
366 phase progression, and cytokinesis. In addition, it has been shown before that PLK1 can affect
367 the activity of cellular transcription factors through several mechanisms. Phosphorylation of the
368 tumor suppressor p53 and the related p73 protein impair the transactivation activity of both
369 transcription factors. In p73, the substrate site of PLK1 has been mapped to the TAD (Ando *et*
370 *al*, 2004; de Carcer, 2019; Koida *et al*, 2008; Martin & Strebhardt, 2006). Phosphorylation of the
371 transcription factor FOXO1 by PLK1 causes its nuclear exclusion and thereby prevents its
372 action (Yuan *et al*, 2014). On the other hand, PLK1 phosphorylation of the transcription factor
373 FoxM1, a critical transactivator of mitotic gene expression, induces FoxM1 activity (Marceau *et*
374 *al*, 2019). It is tempting to speculate that PLK1 might contribute to the general mitotic
375 transcriptional shut down by inhibiting distinct transcription factor activities. In parallel, PLK1
376 might guide the transcriptional activity of the cell to processes relevant to mitotic progression
377 and maintenance of genomic integrity.

378 In healthy immunocompetent hosts, EBNA2 is expressed in a short time window
379 immediately post-infection before either EBNA2 expression is silenced or the EBNA2
380 expressing cell is eliminated by the immune system. Immunodeficient patients, suffering from
381 profound T cell suppression, can develop aggressive EBNA2-positive B cell lymphoproliferative
382 diseases and EBNA2 is a driving force for these tumor entities. The "primary goal" of latent
383 viruses like EBV is to establish a balanced equilibrium of its latent and lytic phase while tumor
384 development is an accident in its life cycle with no benefit for virus dissemination (Shannon-
385 Lowe & Rickinson, 2019). EBNA2 obeys the intracellular signaling cues that silence its activity
386 during a short time window of the cell cycle in order to establish latency and maintain the viral
387 life cycle rather than promoting tumorigenesis. It is well established that high-level expression of
388 PLK1 promotes carcinogenesis in multiple tissues (Liu *et al.*, 2017; Strebhardt, 2010; Strebhardt
389 & Ullrich, 2006). PLK1 is also considered as an oncotarget for aggressive B cell lymphomas
390 since it stabilizes MYC (Ren *et al.*, 2018). Currently, clinical trials evaluate the safety and
391 efficacy of PLK1 inhibitors for patient treatment. However, in some tumor types high-level PLK1
392 expression can suppress cancerogenesis (de Carcer, 2019; Raab *et al.*, 2018).

393 Here we show that PLK1 is an important cellular control factor that restrains the
394 proliferation and transformation of latently infected B cells driven by a growth program that
395 depends on EBNA2. Since two distinct EBNA2 mutants that both target independent PLK1
396 related functions of the EBNA2/PLK1 complex promote cancerogenesis, we conclude that PLK1
397 might act as a tumor suppressor in EBNA2 driven pathogenesis. Based on our results, the
398 development and therapeutic use of PLK1 inhibitors should be re-considered and closely
399 monitored with respect to potential adverse effects in the context of the prevalent latent EBV
400 infections in the population.

401

402

403

404 **MATERIALS AND METHODS**

405 **Cell culture**

406 EBV infected long-term cultures (LCLs), DG75 cells (Ben-Bassat *et al*, 1977), DG75^{Dox HA-EBNA2}
407 (Glaser *et al.*, 2017), Raji (Pulvertaft, 1964), and HEK293 cells were cultured in RPMI 1640
408 supplemented with 10% fetal bovine serum (FBS), 1% non-essential amino acids, 2 mM L-
409 glutamine, 1 mM sodium pyruvate, 100 U/ml penicillin, 100 µg/ml streptomycin, 100 nM sodium
410 selenite and 50µM α-thioglycerols at 37°C in 6% CO₂ atmosphere. Media for HEK293 cells
411 transfected with recombinant EBV and DG75^{Dox HA-EBNA2} contained 1 µg/ml puromycin.

412

413 **Purification of human primary B cell and LCL establishment**

414 Human primary B cells were isolated from adenoid from routine adenoidectomy were obtained
415 from the Department of Otorhinolaryngology, Klinikum Grosshadern, Ludwig Maximilians
416 University of Munich, and Dritter Orden Clinic, Munich-Nymphenburg, Germany. All clinical
417 samples were made fully anonymous. To isolate human primary B cells, T cells were depleted
418 by erythrocyte rosetting using sheep red blood cells and B cells were separated by Ficoll density
419 gradient centrifugation as recommended by the manufacturer (GE Healthcare). The remaining
420 erythrocytes were lysed in red blood cell lysis buffer (155 mM NH₄Cl, 10 mM KHCO₃, 0.1 mM
421 EDTA). Cells were co-stained by anti-CD3⁺ (UCHT1; BD Pharmingen) and anti-CD19⁺(HIB19;
422 BD Pharmingen) antibodies and analyzed by flow cytometry.

423 To generate LCLs, primary human B cells were infected with recombinant EBV at a ratio of 1
424 green raji unit (GRU) to 10 cells for 48 h and cultivated in medium containing 0.5 µg/ml
425 cyclosporine A for 2 weeks before routine cell culture conditions were applied.

426

427 **Antibodies, western blot, immunoprecipitation, and GST-pull down**

428 Monoclonal antibodies specific for His₆ (2F12), EBNA2 (R3), Glutathione S transferase (6G9),
429 HA-tag (3F10), BSA (3C5), LMP1 (1G6) were provided by the antibody facility of the Helmholtz
430 Center Munich. Commercial providers were: GAPDH (Mab374; Merck Millipore), Flag (M2;
431 Sigma Aldrich), PLK1 (ab17056; Abcam), GFP (7.1 and 13.1; Roche) and a p300 specific serum
432 (C20; Santa Cruz). For immunoprecipitations and Western blotting the equivalent of 1x10⁷ cells
433 was lysed in 500 µl of lysis buffer (1% NP40, 10 mM Tris-HCl pH 7.4, 3% glycerol, 150 mM
434 NaCl, 1 mM EDTA) supplemented with cOmplete protease inhibitor and PhoStop phosphatase
435 inhibitor (Roche) incubated for 30 min at 4°C with constant rolling and for 30 min on ice. The
436 lysate was cleared by centrifugation (16000 g, 15 min). 1 µg of purified antibodies or 100 µl of

437 hybridoma supernatants were coupled to Protein A or G beads and added to the cleared lysates,
438 incubated for 2 hours at 4°C, washed with lysis buffer and the protein was eluted with Laemmli
439 buffer. For GST pulldown, antibody coated beads were replaced by GST fusion protein coated
440 beads. 20 µg protein of total cell lysates or 5x10⁶ cell equivalents of one immunoprecipitation
441 were loaded per lane. Signals on Western blots were detected by enhanced
442 chemiluminescence (GE Healthcare) and exposed to films or Fusion FX (Vilber Lourmat).

443

444 **Construction of plasmids**

445 All the plasmid used in the study were cloned based on conventional PCR, restriction digestion,
446 and ligation. Mutated alleles were generated by overlap PCR adapted from the previous
447 protocol (reviewed in Francis *et al*, 2017). In essence of overlap PCR is based on four
448 strategically designed primers. Internally positioned primers must contain complementary
449 sequences to each other, and both of them must contain the mutation of interest, like a
450 substitution, a deletion, or an insertion. The flanking primers might contain restriction enzyme
451 recognition sites to facilitate the cloning of the amplified fragment. Two steps were performed, in
452 the first round of PCR reactions using the forward primer of the flanking primers with the reverse
453 primer of the internally positioned primers and vice versa, respectively. The resulting amplified
454 short fragments worked as templates when mixed with the flanking primer pairs, which results in
455 amplification of the final long fragment with the desired mutation in the second round of PCR.
456 The second PCR product is digested and inserted into a corresponding vector. For each
457 plasmid used in the study detail information about primer pairs, template, and vector is shown in
458 Table S1.

459

460 **Expression and purification of His- or GST-tagged proteins**

461 His₆-tagged and GST-tagged proteins were expressed in E. coli Rosetta (DE3) cells and purified
462 according to manufacturer's instructions using Ni-chelate agarose (Quiagen) or glutathione
463 coupled Sepharose 4B beads (GE Healthcare).

464

465 **Kinase assay in vitro**

466 Purified protein or protein coupled to beads were incubated for 30 min at 37°C with recombinant
467 active Cyclin B/CDK1 (100 ng) or PLK1 (50 ng) in the presence of 1mM normal ATP or plus
468 0.25 mCi/ml γ -³²P labeled ATP in PK buffer (50 mM Tris-HCl, 10 mM MgCl₂, 0.1 mM EDTA, 2
469 mM DTT, 0.01% Brij 35, pH 7.5) in a total reaction volume of 20 µl.

470

471 **EBV BAC recombineering**

472 All recombinant EBV strains used in this study were generated by a two-step selection protocol
473 using the λ -prophage-based heat inducible Red recombination system expressed in *E. coli*
474 strain SW105 (Pich *et al.*, 2019; Wang *et al.*, 2009; Warming *et al.*, 2005). For the first step, a
475 Kan/rpsL expression cassette was flanked by 50 nt EBV sequences of the respective EBNA2
476 gene locus by PCR using the template p6012. The resulting PCR product was used to insert the
477 Kan/rpsL cassette by homologous recombination into the specific EBV/EBNA2 target site by
478 transformation and kanamycin (30 $\mu\text{g/ml}$) and chloramphenicol (12.5 $\mu\text{g/ml}$) selection of SW105
479 pre-transformed with the recombinant target EBV plasmid. As a second step, a synthetic DNA
480 fragment or PCR product carrying the desired mutation flanked by ~ 300 nt of the genomic viral
481 sequence was used to replace the Kan/rpsL cassette by homologous recombination to generate
482 the final mutant EBV plasmid by streptomycin (1 mg/ml) and chloramphenicol (12.5 $\mu\text{g/ml}$)
483 selection. For each BACmid used in the study, detailed information about primer pairs, template,
484 and vector are shown in Table S1.

485

486 **Production of recombinant virus**

487 HEK293 transfectants carrying the recombinant virus plasmid were induced for virus production
488 by co-transfection of 0.5 μg of the plasmids p509 encoding BZLF1 and p2670 encoding BALF4
489 per one 6-well in 3 ml cell cultures. The supernatants of the transfectants were harvested 3 days
490 post-transfection and passed through a 0.8 μm filter. For quantification of viral titers, 1×10^5 Raji
491 cells were infected with serial dilutions of viral supernatants in 2 ml cultures and the percentage
492 of GFP positive cells was determined by FACS analysis 3 days post-infection. The
493 concentration of viral stocks was expressed as the number of green Raji units (GRU).

494

495 **Isothermal titration calorimetry**

496 Experiments were performed on a ITC200 instrument in triplicates and analyzed with the
497 Malvern software. 100 μM PBD was provided in the cell and titrated with 1 mM concentration of
498 wild type ((PNTSSPS) or phosphopeptide (PNTSpSPS) with 25 times 1.5 μL injections at 25°C.

499

500 **Generation and infection of humanized mice**

501 NOD scid $\gamma_c^{-/-}$ (NSG) mice obtained from the Jackson Laboratories were bred and maintained
502 under specific pathogen-free conditions at the Institute of Experimental Immunology, University
503 of Zurich. CD34⁺ human hematopoietic progenitor cells were isolated from human fetal liver
504 tissue (obtained from Advanced Bioscience Resources) using the CD34 MicroBead Kit (Miltenyi

505 Biotec) following the protocol provided by the manufacturer. Newborn NSG mice (age: 1 to 5
506 days) were irradiated with 1 Gy by use of an x-ray source. $1 - 3 \times 10^5$ CD34⁺ human
507 hematopoietic progenitor cells were injected intrahepatically 5 to 7 hours after irradiation.
508 Reconstitution of mice with human immune system components was investigated 10 – 12
509 weeks after engraftment by flow cytometry for the cell surface expression of huCD45 (BV605 or
510 Pacific Blue, clone HI30; Biolegend), huCD3 (PE, clone UCHT1; BV785, clone OKT3;
511 Biolegend), huCD19 (PE-Cy7, clone HIB19; Biolegend) and (PE-Texas Red, Clone SJ25-C1),
512 huCD4 (APC-Cy7, clone RPA-T4; Biolegend), huCD8 (PerCP, clone SK1; Biolegend), huNKp46
513 (APC, clone 9E2; BD) and HLA-DR (FITC or PE-Cy7 clone L243; Biolegend) on PBMCs. 12 -
514 16 weeks after engraftment, humanized mice were infected intraperitoneally with 1×10^5 GRU of
515 EBV wt, EBV S379A or EBV S457A/T465V. For each experiment, a different cohort of mice
516 reconstituted with CD34⁺ cells derived from one donor was generated. The animals were
517 ascribed to a distinct experimental group ensuring similar ratios of males to females and similar
518 reconstitution levels and immune cell activation in the peripheral blood. 5 weeks after infection
519 mice were sacrificed if not necessitated earlier by the regulations of our experimental animal
520 license as a consequence of general health conditions or weight loss over 20%. For analysis of
521 the experiments, only those mice that showed two of the following signs of infection were
522 regarded as infected and included in the analysis: (i) Viral loads in spleen, (ii) viral loads in
523 blood at one time-point during the experiment, (iii) EBNA2⁺ cells in spleen as evaluated by
524 histology. The respective animal protocol (ZH159-17/ZH008-20) was approved by the veterinary
525 office of the canton of Zurich, Switzerland.

526

527 **Whole blood and spleen preparations for immune phenotyping**

528 Whole blood of mice was collected from the tail vein and prepared for immunophenotyping by
529 lysing erythrocytes with NH₄Cl. Spleens of mice were mashed, subsequently filtered with a 70
530 µm cell strainer, and afterwards mononuclear cells were separated using Ficoll-Paque gradients.
531 Total cell counts were determined from purified mononuclear cell suspensions using a DxH500
532 Hematology Analyzer (Beckman Coulter). Purified cell suspensions were stained for 30 – 40
533 minutes at 4°C in the dark with a master mix of the respective antibodies followed by a washing
534 step in PBS. The stained cells were analyzed in an LSR Fortessa cytometer (BD Biosciences).
535 Flow cytometry data were analyzed using the FlowJo software.

536

537 **EBV DNA Quantification in Tissue**

538 Total DNA from splenic tissue and whole blood was extracted using DNeasy Blood & Tissue Kit
539 (QIAGEN) and NucliSENS (bioMérieux), respectively, according to manufacturer's instructions.
540 Quantitative analysis of EBV DNA in humanized mouse spleens and blood was performed by a
541 TaqMan (Applied Biosystems) real-time PCR as described previously (Berger et al., 2001) with
542 modified primers (5'-CTTCTCAGTCCAGCGCGTTT-3' and 5'-CAGTGGTCCCCCTCCCTAGA-3')
543 and the fluorogenic probe (5'-(FAM)-CGTAAGCCAGACAGCAGCCAATTGTCAG-(TAMRA)-3')
544 for the amplification of a 70-base pair sequence in the conserved BamHI W fragment of EBV.
545 Real-time PCR was run on a ViiA 7 Realtime PCR system or a CFX384 Touch Real-Time PCR
546 Detection System and samples were analyzed in duplicates.

547

548 **IgV gene rearrangement sequence analysis**

549 For PCR analysis of rearranged immunoglobulin genes, macroscopically visible tumors were
550 dissected and cryofixedated in Tissue Tek® O.C.T.™ (VWR, Cat# SAKU4583) on dry ice.

551 DNA was isolated from 10-20 8-µm frozen tissue sections of biopsies from humanized mice
552 using the PureGene DNA isolation kit (Qiagen, Hilden, Germany). PCR was performed with six
553 framework region 1 subgroup specific primers and a JH primer mix (3' JH mix) for 35 cycles in
554 six separate reactions, using 300 ng of DNA per reaction. Primer sequences have been
555 published before (Kuppers *et al*, 2019). PCR products were purified from agarose gels and
556 Sanger sequenced with the IGHV primers used for PCR and the BigDye Sequencing Kit (ABI,
557 Heidelberg, Germany) on an Applied Biosystems 3130 Genetic Analyzer (ABI). Sequences
558 were evaluated with the IMGT/V-Quest software (http://www.imgt.org/IMGT_vquest/input).

559

560 **Mass Spectrometry of EBNA2 co-immunoprecipitates**

561 DG75 cells were transfected with a C-terminal HA-tagged EBNA2 (plasmid: pAG155) using
562 electroporation. After 48 h, cells were lysed in NP-40 lysis buffer (1% NP40, 10 mM Tris-HCl pH
563 7.4, 3% glycerol, 150 mM NaCl, 1 mM EDTA supplemental with cOmplete protease and
564 PhoStop phosphatase inhibitor). Cell debris was depleted by centrifugation. The cell extract was
565 incubated with protein G beads covalently coupled with an HA-specific antibody.
566 Immunoprecipitates were eluted with Lämmeli buffer.

567 After reduction and alkylation using DTT and IAA, the proteins were centrifuged on a 30 kDa
568 cutoff filter device, washed thrice with UA buffer (8 M urea in 0.1 M Tris/HCl pH 8.5) and twice
569 with 50 mM ammonium bicarbonate. The proteins were digested for 16 h at 37°C using 1 µg
570 trypsin. After centrifugation (10 min at 14,000× g), the eluted peptides were acidified with 0.5%
571 Trifluoroacetic acid and stored at -20°C.

572 LC-MS/MS analysis was performed on a LTQ Orbitrap XL mass spectrometer (Thermo
573 Scientific, Waltham, MA, USA) online coupled to an Ultimate 3000 nano-RSLC (Thermo
574 Scientific). Tryptic peptides were automatically loaded on a C18 trap column (300 μm inner
575 diameter (ID) \times 5 mm, Acclaim PepMap100 C18, 5 μm , 100 \AA , LC Packings) prior to C18
576 reversed phase chromatography on the analytical column (Acclaim PepMap C18, 50 μm ID \times
577 250 mm, 2 μm , 100 \AA , LC Packings) at 300 nL/min flow rate in a 140 min acetonitrile gradient
578 from 4 to 30% in 0.1% formic acid. Profile precursor spectra from 300 to 1500 m/z were
579 recorded in the orbitrap with a maximum injection time of 500 ms. TOP10 fragment spectra of
580 charges 2 to 7 were recorded in the linear ion trap with a maximum injection time of 100 ms, an
581 isolation window of 2.0 m/z, a normalized collision energy of 35 and a dynamic exclusion of 60 s.
582 Raw files were analyzed using Progenesis QI for proteomics (version 2.0, Nonlinear Dynamics,
583 part of Waters). Features of charges 2–7 were used and all MS/MS spectra were exported as
584 mgf file. Peptide searches were performed using Mascot search engine (version 2.5.1) against
585 the Ensembl Human protein database (100158 sequences, 37824871 residues). Search
586 settings were: 10 ppm precursor tolerance, 0.6 Da fragment tolerance, one missed cleavage
587 allowed. Carbamidomethyl on cysteine was set as a fixed modification, deamidation of
588 glutamine and asparagine allowed as variable modification, as well as oxidation of methionine.
589 Applying the percolator algorithm with a cut-off of 13 and $p < 0.05$ resulted in a peptide false
590 discovery rate (FDR) of 1.54%. Search results were reimported in the Progenesis QI software.
591 Proteins were quantified by summing up the abundances of all unique peptides per protein.
592 Resulting protein abundances were used for the calculation of fold-changes and statistics
593 values.

594

595 **Mass Spectrometry on purified EBNA2 phosphorylated by PLK1 in vitro**

596 EBNA2 and GST-fused EBNA2 proteins, purified from bacteria, were subjected to PLK1 kinase
597 assays. 50 μg EBNA2 or 130 μg GST-fused EBNA2 protein were incubate in 1x PK buffer (NEB,
598 50 mM Tris-HCl, 10 mM MgCl_2 , 0.1 mM EDTA, 2 mM DTT, 0.01% Brij 35, pH 7.5), 1.25 mM
599 ATP in presence or absence of 250 ng active PLK1 (SignalChem) at 37°C for 1 h. All reactions
600 were carried out in a total volume of 20 μL and then were quenched with 5 μL 5x Lämmli
601 sample buffer.

602 Proteins were separated by SDS-PAGE, and stained with Coomassie colloidal blue. Bands
603 corresponding to EBNA2 full length (86 kD) or GST-EBNA2 C-terminal fragment (28 kD) were
604 sliced out from the gel lane, and proteins were then reduced, alkylated, and digested with either
605 trypsin or GluC (Roche), as previously described (Shevchenko *et al.*, 1996).

606 Dried peptides were reconstituted in 0.1% FA/2% ACN and subjected to MS analysis using a
607 Dionex Ultimate 3000 UHPLC+ system coupled to a Fusion Lumos Tribrid mass spectrometer
608 (Thermo Fisher). Peptides were delivered to a trap column (75 μm \times 2 cm, packed in-house with
609 5 μm Reprosil C18 resin; Dr. Maisch) and washed using 0.1% FA at a flow rate of 5 $\mu\text{L}/\text{min}$ for
610 10 min. Subsequently, peptides were transferred to an analytical column (75 μm \times 45 cm,
611 packed in-house with 3 μm Reprosil C18 resin, Dr. Maisch) applying a flow rate of 300 nL/min.
612 Peptides were chromatographically separated using a 50 min linear gradient from 4% to 32%
613 solvent B (0.1% FA, 5% DMSO in ACN) in solvent A (0.1% FA in 5% DMSO). The mass
614 spectrometer was operated in data-dependent mode, automatically switching between MS and
615 MS/MS. Full-scan MS spectra (from m/z 360 to 1500) were acquired in the Orbitrap with a
616 resolution of 60,000 at m/z 200, using an automatic gain control (AGC) target value of 5e5
617 charges and maximum injection time (maxIT) of 10 ms. The 10 most intense ions within the
618 survey scan were selected for HCD fragmentation with normalized collision energy set to 28%.
619 Isolation window was set to 1.7 Th, and MS/MS spectra were acquired in the Orbitrap with a
620 resolution of 15,000 at m/z 200, using an AGC target value of 2e5, and a maxIT of 75 ms.
621 Dynamic exclusion was set to 20 s.

622 Peptide and protein identification was performed using MaxQuant (version 1.5.3.30) with its built
623 in search engine Andromeda (Cox & Mann, 2008). Spectra were searched against a SwissProt
624 database, either the *Spodoptera frugiperda* (OX 7108 - 26,502 sequences) or *Escherichia coli*
625 (UP000002032 – 4,156 sequences), supplemented with the EBNA2 protein sequence. Enzyme
626 specificity was set to Trypsin/P or GluC accordingly, and the search included cysteine
627 carbamidomethylation as a fixed modification, protein N-term acetylation, oxidation of
628 methionine, and phosphorylation of serine, threonine, tyrosine residue (STY) as variable
629 modifications. Up to two and three missed cleavage sites were allowed for trypsin and GluC,
630 respectively. Precursor tolerance was set to 4.5 ppm (after MS1 feature re-calibration), and
631 fragment ion tolerance to 20 ppm. The match between runs feature was enable. Peptides
632 identification were further filtered for a minimum Andromeda score of 20 or 40, for unmodified
633 and modified (phosphorylated) sequences, respectively. A site localization probability of at least
634 0.75 was used as the threshold for confident localization (Vizcaino *et al*, 2013; Vizcaino *et al*,
635 2016).

636

637 **Cell proliferation assay**

638 Human adenoid primary B cells were stained with CellTrace Violet according to the
639 manufacturer's instructions (Thermo Fisher Scientific). Proliferation of CD19⁺ B cells was

640 monitored by flow cytometry using BD Fortessa and the data were analyzed using the FlowJo
641 software (Version 10.5.3).

642

643 **Dual luciferase assay**

644 5×10^6 DG75 cells were electroporated with 1.5 μg EBNA2 expression plasmids and the
645 luciferase construct 1.5 μg pGa981.6 (Minoguchi *et al.*, 1997) carrying a multimerized CBF1
646 binding site to measure EBNA2 activity and 0.2 μg renilla luciferase expression plasmid. 24 h
647 post electroporation, cells were washed, pelleted and lysed in 100 μL lysis buffer for 30 min on
648 ice. Cell extracts were tested by the dual luciferase assay according to the manufacturer's
649 instructions (Promega).

650

651

652 **RESOURCES**

653 **Data Availability**

654 Phosphorylation of EBNA2 by PLK1:

655 The mass spectrometry proteomics data have been deposited in the ProteomeXchange
656 Consortium via the PRIDE partner repository (Link: <https://www.ebi.ac.uk/pride/login> -
657 Username: reviewer_pxd022970@ebi.ac.uk - Password: wZd0Qfaz) with the dataset
658 identifier PXD022970 (Vizcaino *et al.*, 2013; Vizcaino *et al.*, 2016).

659

660

661 **ACKNOWLEDGEMENT**

662 We thank Dagmar Pich, Yen-Fu Adam Chen, Ezgi Akidil for all the excellent advice they gave.

663 We thank Kerstin Heise, Michaela Kroetz-Fahning and Andreas Klaus for expert technical
664 assistance. This project was supported by the Wilhelm Sander-Stiftung (Grant 2015.165.1) to
665 Bettina Kempkes. Xiang Zhang is supported by the China Scholarship Council (CSC No.:
666 201603250052). Cristian Münz is financially supported by Cancer Research Switzerland (KFS-
667 4091-02-2017 and KFS-4962-02-2020), KFSP-PrecisionMS and HMZ ImmunoTargET of the
668 University of Zurich, the Cancer Research Center Zurich, the Vontobel Foundation, the
669 Baugarten Foundation, the Sobek Foundation, the Swiss Vaccine Research Institute, Roche,
670 Novartis and the Swiss National Science Foundation (310030B_182827, 310030L_197952/1
671 and CRSII5_180323)

672

673

674 **AUTHOR CONTRIBUTIONS**

675 Conceptualization: XZ, MS, CM, RK, BKe; Formal analysis and data curation: AMo, PG, SMH,
676 Methodology: XZ, PS, MR, KS, CM; Funding acquisition: BKe, CM; Investigation: XZ, PS, AMo,
677 PG, AMu, ST, CKR, SB, RK; Resources: WH, MR, MS, CM, KS, BKu, CM; Supervision: WH,
678 RK, MS, CM, BKe; Visualization: XZ, PS, AMo; BKe; Writing –original draft: XZ, BKe; Writing-
679 review&editing: XZ, MS, CM, PG, PS, AMo , BKe; RK;

680

681 **CONFLICT OF INTEREST**

682 The authors declare no conflict of interest.

683

684 **REFERENCES**

685 Ando K, Ozaki T, Yamamoto H, Furuya K, Hosoda M, Hayashi S, Fukuzawa M, Nakagawara A
686 (2004) Polo-like kinase 1 (Plk1) inhibits p53 function by physical interaction and
687 phosphorylation. *The Journal of biological chemistry* 279: 25549-25561
688 Barr FA, Sillje HH, Nigg EA (2004) Polo-like kinases and the orchestration of cell division.
689 *Nature reviews Molecular cell biology* 5: 429-440
690 Ben-Bassat H, Goldblum N, Mitrani S, Goldblum T, Yoffey JM, Cohen MM, Bentwich Z, Ramot
691 B, Klein E, Klein G (1977) Establishment in continuous culture of a new type of lymphocyte from
692 a "Burkitt like" malignant lymphoma (line D.G.-75). *Int J Cancer* 19: 27-33
693 Caduff N, McHugh D, Murer A, Rämmer P, Raykova A, Landtwing V, Rieble L, Keller CW,
694 Prummer M, Hoffmann L *et al* (2020) Immunosuppressive FK506 treatment leads to more
695 frequent EBV-associated lymphoproliferative disease in humanized mice. *PLoS pathogens* 16:
696 e1008477
697 Chabot PR, Raiola L, Lussier-Price M, Morse T, Arseneault G, Archambault J, Omichinski JG
698 (2014) Structural and functional characterization of a complex between the acidic transactivation
699 domain of EBNA2 and the Tfb1/p62 subunit of TFIIH. *PLoS pathogens* 10: e1004042
700 Cheng K-Y, Lowe ED, Sinclair J, Nigg EA, Johnson LN (2003) The crystal structure of the
701 human polo-like kinase-1 polo box domain and its phospho-peptide complex. *The EMBO journal*
702 22: 5757-5768
703 Cohen JI (1992) A region of herpes simplex virus VP16 can substitute for a transforming domain
704 of Epstein-Barr virus nuclear protein 2. *Proceedings of the National Academy of Sciences of the*
705 *United States of America* 89: 8030-8034
706 Cohen JI, Kieff E (1991) An Epstein-Barr virus nuclear protein 2 domain essential for
707 transformation is a direct transcriptional activator. *Journal of virology* 65: 5880-5885.
708 Cohen JI, Wang F, Kieff E (1991) Epstein-Barr virus nuclear protein 2 mutations define essential
709 domains for transformation and transactivation. *Journal of virology* 65: 2545-2554
710 Cox J, Mann M (2008) MaxQuant enables high peptide identification rates, individualized p.p.b.-
711 range mass accuracies and proteome-wide protein quantification. *Nature biotechnology* 26:
712 1367-1372
713 de Carcer G (2019) The Mitotic Cancer Target Polo-Like Kinase 1: Oncogene or Tumor
714 Suppressor? *Genes* 10
715 Elia AE, Cantley LC, Yaffe MB (2003a) Proteomic screen finds pSer/pThr-binding domain
716 localizing Plk1 to mitotic substrates. *Science* 299: 1228-1231

717 Elia AE, Rellos P, Haire LF, Chao JW, Ivins FJ, Hoepker K, Mohammad D, Cantley LC,
718 Smerdon SJ, Yaffe MB (2003b) The molecular basis for phosphodependent substrate targeting
719 and regulation of Plks by the Polo-box domain. *Cell* 115: 83-95
720 Farrell CJ, Lee JM, Shin EC, Cebrat M, Cole PA, Hayward SD (2004) Inhibition of Epstein-Barr
721 virus-induced growth proliferation by a nuclear antigen EBNA2-TAT peptide. *Proceedings of the*
722 *National Academy of Sciences of the United States of America* 101: 4625-4630
723 Farrell PJ (2019) Epstein-Barr Virus and Cancer. *Annual review of pathology* 14: 29-53
724 Francis MS, Amer AAA, Milton DL, Costa TRD (2017) Site-Directed Mutagenesis and Its
725 Application in Studying the Interactions of T3S Components. In: *Type 3 Secretion Systems:*
726 *Methods and Protocols*, Nilles M.L., Condry D.L.J. (eds.) pp. 11-31. Springer New York: New
727 York, NY
728 Friberg A, Thumann S, Hennig J, Zou P, Nossner E, Ling PD, Sattler M, Kempkes B (2015) The
729 EBNA-2 N-Terminal Transactivation Domain Folds into a Dimeric Structure Required for Target
730 Gene Activation. *PLoS pathogens* 11: e1004910
731 Gheghiani L, Loew D, Lombard B, Mansfeld J, Gavet O (2017) PLK1 Activation in Late G2 Sets
732 Up Commitment to Mitosis. *Cell Rep* 19: 2060-2073
733 Glaser LV, Rieger S, Thumann S, Beer S, Kuklik-Roos C, Martin DE, Maier KC, Harth-Hertle
734 ML, Gruning B, Backofen R *et al* (2017) EBF1 binds to EBNA2 and promotes the assembly of
735 EBNA2 chromatin complexes in B cells. *PLoS pathogens* 13: e1006664
736 Harter MR, Liu CD, Shen CL, Gonzalez-Hurtado E, Zhang ZM, Xu M, Martinez E, Peng CW,
737 Song J (2016) BS69/ZMYND11 C-Terminal Domains Bind and Inhibit EBNA2. *PLoS pathogens*
738 12: e1005414
739 Henkel T, Ling PD, Hayward SD, Peterson MG (1994) Mediation of Epstein-Barr virus EBNA2
740 transactivation by recombination signal-binding protein J kappa. *Science* 265: 92-95
741 Hsieh JJ, Hayward SD (1995) Masking of the CBF1/RBPJ kappa transcriptional repression
742 domain by Epstein-Barr virus EBNA2. *Science* 268: 560-563
743 Kempkes B, Ling PD (2015) EBNA2 and Its Coactivator EBNA-LP. *Current topics in*
744 *microbiology and immunology* 391: 35-59
745 Koida N, Ozaki T, Yamamoto H, Ono S, Koda T, Ando K, Okoshi R, Kamijo T, Omura K,
746 Nakagawara A (2008) Inhibitory role of Plk1 in the regulation of p73-dependent apoptosis
747 through physical interaction and phosphorylation. *The Journal of biological chemistry* 283: 8555-
748 8563
749 Kuppers R, Schneider M, Hansmann ML (2019) Laser-Based Microdissection of Single Cells
750 from Tissue Sections and PCR Analysis of Rearranged Immunoglobulin Genes from Isolated
751 Normal and Malignant Human B Cells. *Methods Mol Biol* 1956: 61-75
752 Kuppers R, Zhao M, Rajewsky K, Hansmann ML (1993) Detection of clonal B cell populations in
753 paraffin-embedded tissues by polymerase chain reaction. *Am J Pathol* 143: 230-239
754 Kwiatkowski B, Chen SY, Schubach WH (2004) CKII site in Epstein-Barr virus nuclear protein 2
755 controls binding to hSNF5/Ini1 and is important for growth transformation. *Journal of virology* 78:
756 6067-6072
757 Lee KH, Hwang J-A, Kim S-O, Kim JH, Shin SC, Kim EE, Lee KS, Rhee K, Jeon BH, Bang JK
758 *et al* (2018) Phosphorylation of human enhancer filamentation 1 (HEF1) stimulates interaction
759 with Polo-like kinase 1 leading to HEF1 localization to focal adhesions. *The Journal of biological*
760 *chemistry* 293: 847-862
761 Lee KS, Park JE, Kang YH, Kim TS, Bang JK (2014) Mechanisms underlying Plk1 polo-box
762 domain-mediated biological processes and their physiological significance. *Molecules and cells*
763 37: 286-294
764 Ling PD, Hayward SD (1995) Contribution of conserved amino acids in mediating the interaction
765 between EBNA2 and CBF1/RBPJk. *Journal of virology* 69: 1944-1950.
766 Liu Z, Sun Q, Wang X (2017) PLK1, A Potential Target for Cancer Therapy. *Translational*
767 *oncology* 10: 22-32

768 Longnecker RM, Kieff E, Cohen JI (2013) Epstein-Barr virus. In: *Fields Virology*, Knipe D.M.,
769 Howley P.M., Cohen J.I., Griffin D.E., Lamb R.A., Martin M.A., Racianello V.R., Roizman B.
770 (eds.) pp. 1898-1959. Lippincott Williams and Wilkins: Philadelphia
771 Lowery DM, Lim D, Yaffe MB (2005) Structure and function of Polo-like kinases. *Oncogene* 24:
772 248-259
773 Lu F, Chen HS, Kossenkov AV, DeWiseleare K, Won KJ, Lieberman PM (2016) EBNA2 Drives
774 Formation of New Chromosome Binding Sites and Target Genes for B-Cell Master Regulatory
775 Transcription Factors RBP-jkappa and EBF1. *PLoS pathogens* 12: e1005339
776 Marceau AH, Brison CM, Nerli S, Arsenault HE, McShan AC, Chen E, Lee HW, Benanti JA,
777 Sgourakis NG, Rubin SM (2019) An order-to-disorder structural switch activates the FoxM1
778 transcription factor. *eLife* 8
779 Martin BT, Strebhardt K (2006) Polo-like kinase 1: target and regulator of transcriptional control.
780 *Cell cycle* 5: 2881-2885
781 Minoguchi S, Taniguchi Y, Kato H, Okazaki T, Strobl LJ, Zimmer-Strobl U, Bornkamm GW,
782 Honjo T (1997) RBP-L, a transcription factor related to RBP-Jkappa. *Molecular and cellular*
783 *biology* 17: 2679-2687
784 Mrozek-Gorska P, Buschle A, Pich D, Schwarzmayr T, Fechtner R, Scialdone A,
785 Hammerschmidt W (2019) Epstein-Barr virus reprograms human B lymphocytes immediately in
786 the prelatent phase of infection. *Proceedings of the National Academy of Sciences of the United*
787 *States of America* 116: 16046-16055
788 Munz C (2019) Latency and lytic replication in Epstein-Barr virus-associated oncogenesis. *Nat*
789 *Rev Microbiol* 17: 691-700
790 Nakajima H, Toyoshima-Morimoto F, Taniguchi E, Nishida E (2003) Identification of a
791 consensus motif for Plk (Polo-like kinase) phosphorylation reveals Myt1 as a Plk1 substrate.
792 *The Journal of biological chemistry* 278: 25277-25280
793 Pavlovsky AG, Liu X, Faehnle CR, Potente N, Viola RE (2012) Structural characterization of
794 inhibitors with selectivity against members of a homologous enzyme family. *Chem Biol Drug*
795 *Des* 79: 128-136
796 Pich D, Mrozek-Gorska P, Bouvet M, Sugimoto A, Akidil E, Grundhoff A, Hamperl S, Ling PD,
797 Hammerschmidt W (2019) First Days in the Life of Naive Human B Lymphocytes Infected with
798 Epstein-Barr Virus. *MBio* 10
799 Ponnusamy R, Khatri R, Correia PB, Wood CD, Mancini EJ, Farrell PJ, West MJ (2019)
800 Increased association between Epstein-Barr virus EBNA2 from type 2 strains and the
801 transcriptional repressor BS69 restricts EBNA2 activity. *PLoS pathogens* 15: e1007458
802 Pulvertaft JV (1964) Cytology of Burkitt's Tumour (African Lymphoma). *Lancet* 39: 238-240
803 Raab M, Sanhaji M, Matthess Y, Horlin A, Lorenz I, Dotsch C, Habbe N, Waidmann O, Kurunci-
804 Csacsko E, Firestein R *et al* (2018) PLK1 has tumor-suppressive potential in APC-truncated
805 colon cancer cells. *Nature communications* 9: 1106
806 Rajewsky K (1996) Clonal selection and learning in the antibody system. *Nature* 381: 751-758
807 Ren Y, Bi C, Zhao X, Lwin T, Wang C, Yuan J, Silva AS, Shah BD, Fang B, Li T *et al* (2018)
808 PLK1 stabilizes a MYC-dependent kinase network in aggressive B cell lymphomas. *The Journal*
809 *of clinical investigation* 128: 5517-5530
810 Rodel F, Zhou S, Gyorffy B, Raab M, Sanhaji M, Mandal R, Martin D, Becker S, Strebhardt K
811 (2020) The Prognostic Relevance of the Proliferation Markers Ki-67 and Plk1 in Early-Stage
812 Ovarian Cancer Patients With Serous, Low-Grade Carcinoma Based on mRNA and Protein
813 Expression. *Front Oncol* 10: 558932
814 Rosenblum D, Gutkin A, Kedmi R, Ramishetti S, Veiga N, Jacobi AM, Schubert MS, Friedmann-
815 Morvinski D, Cohen ZR, Behlke MA *et al* (2020) CRISPR-Cas9 genome editing using targeted
816 lipid nanoparticles for cancer therapy. *Science Advances* 6: eabc9450
817 Shannon-Lowe C, Rickinson A (2019) The Global Landscape of EBV-Associated Tumors. *Front*
818 *Oncol* 9: 713

- 819 Shevchenko A, Wilm M, Vorm O, Mann M (1996) Mass spectrometric sequencing of proteins
820 silver-stained polyacrylamide gels. *Anal Chem* 68: 850-858
- 821 Shultz LD, Saito Y, Najima Y, Tanaka S, Ochi T, Tomizawa M, Doi T, Sone A, Suzuki N,
822 Fujiwara H *et al* (2010) Generation of functional human T-cell subsets with HLA-restricted
823 immune responses in HLA class I expressing NOD/SCID/IL2r gamma(null) humanized mice.
824 *Proceedings of the National Academy of Sciences of the United States of America* 107: 13022-
825 13027
- 826 Śledź P, Lang S, Stubbs CJ, Abell C (2012) High-throughput interrogation of ligand binding
827 mode using a fluorescence-based assay. *Angewandte Chemie (International ed in English)* 51:
828 7680-7683
- 829 Strebhardt K (2010) Multifaceted polo-like kinases: drug targets and antitargets for cancer
830 therapy. *Nat Rev Drug Discov* 9: 643-660
- 831 Strebhardt K, Ullrich A (2006) Targeting polo-like kinase 1 for cancer therapy. *Nat Rev Cancer*
832 6: 321-330
- 833 Strowig T, Gurer C, Ploss A, Liu Y-F, Arrey F, Sashihara J, Koo G, Rice CM, Young JW,
834 Chadburn A *et al* (2009a) Priming of protective T cell responses against virus-induced tumors in
835 mice with human immune system components. *The Journal of experimental medicine* 206:
836 1423-1434
- 837 Strowig T, Gurer C, Ploss A, Liu YF, Arrey F, Sashihara J, Koo G, Rice CM, Young JW,
838 Chadburn A *et al* (2009b) Priming of protective T cell responses against virus-induced tumors in
839 mice with human immune system components. *The Journal of experimental medicine* 206:
840 1423-1434
- 841 Thorley-Lawson DA, Gross A (2004) Persistence of the Epstein-Barr virus and the origins of
842 associated lymphomas. *N Engl J Med* 350: 1328-1337
- 843 Tong X, Drapkin R, Reinberg D, Kieff E (1995a) The 62- and 80-kDa subunits of transcription
844 factor IIH mediate the interaction with Epstein-Barr virus nuclear protein 2. *Proceedings of the*
845 *National Academy of Sciences of the United States of America* 92: 3259-3263.
- 846 Tong X, Drapkin R, Yalamanchili R, Mosialos G, Kieff E (1995b) The Epstein-Barr virus nuclear
847 protein 2 acidic domain forms a complex with a novel cellular coactivator that can interact with
848 TFIIIE. *Molecular and cellular biology* 15: 4735-4744.
- 849 Tong X, Wang F, Thut CJ, Kieff E (1995c) The Epstein-Barr virus nuclear protein 2 acidic
850 domain can interact with TFIIIB, TAF40, and RPA70 but not with TATA-binding protein. *Journal*
851 *of virology* 69: 585-588.
- 852 Vizcaino JA, Cote RG, Csordas A, Dianes JA, Fabregat A, Foster JM, Griss J, Alpi E, Birim M,
853 Contell J *et al* (2013) The PRoteomics IDentifications (PRIDE) database and associated tools:
854 status in 2013. *Nucleic acids research* 41: D1063-1069
- 855 Vizcaino JA, Csordas A, Del-Toro N, Dianes JA, Griss J, Lavidas I, Mayer G, Perez-Riverol Y,
856 Reisinger F, Ternent T *et al* (2016) 2016 update of the PRIDE database and its related tools.
857 *Nucleic acids research* 44: 11033
- 858 Wang L, Grossman SR, Kieff E (2000) Epstein-Barr virus nuclear protein 2 interacts with p300,
859 CBP, and PCAF histone acetyltransferases in activation of the LMP1 promoter. *Proceedings of*
860 *the National Academy of Sciences of the United States of America* 97: 430-435.
- 861 Wang S, Zhao Y, Leiby M, Zhu J (2009) A new positive/negative selection scheme for precise
862 BAC recombineering. *Mol Biotechnol* 42: 110-116
- 863 Warming S, Costantino N, Court DL, Jenkins NA, Copeland NG (2005) Simple and highly
864 efficient BAC recombineering using galK selection. *Nucleic acids research* 33: e36
- 865 Watanabe N, Arai H, Iwasaki J, Shiina M, Ogata K, Hunter T, Osada H (2005) Cyclin-dependent
866 kinase (CDK) phosphorylation destabilizes somatic Wee1 via multiple pathways. *Proceedings of*
867 *the National Academy of Sciences of the United States of America* 102: 11663-11668
- 868 West MJ (2017) Chromatin reorganisation in Epstein-Barr virus-infected cells and its role in
869 cancer development. *Current opinion in virology* 26: 149-155

870 Wolf G, Elez R, Doermer A, Holtrich U, Ackermann H, Stutte HJ, Altmannsberger H-M,
871 Rübnsamen-Waigmann H, Strebhardt K (1997) Prognostic significance of polo-like kinase (PLK)
872 expression in non-small cell lung cancer. *Oncogene* 14: 543-549
873 Yuan C, Wang L, Zhou L, Fu Z (2014) The function of FOXO1 in the late phases of the cell
874 cycle is suppressed by PLK1-mediated phosphorylation. *Cell cycle* 13: 807-819
875 Yuan J, Eckerdt F, Bereiter-Hahn J, Kurunci-Csacsco E, Kaufmann M, Strebhardt K (2002)
876 Cooperative phosphorylation including the activity of polo-like kinase 1 regulates the subcellular
877 localization of cyclin B1. *Oncogene* 21: 8282-8292
878 Yuan J, Horlin A, Hock B, Stutte HJ, Rübnsamen-Waigmann H, Strebhardt K (1997) Polo-like
879 kinase, a novel marker for cellular proliferation. *Am J Pathol* 150: 1165-1172
880 Yue W, Davenport MG, Shackelford J, Pagano JS (2004) Mitosis-specific hyperphosphorylation
881 of Epstein-Barr virus nuclear antigen 2 suppresses its function. *Journal of virology* 78: 3542-
882 3552
883 Yue W, Gershburg E, Pagano JS (2005) Hyperphosphorylation of EBNA2 by Epstein-Barr virus
884 protein kinase suppresses transactivation of the LMP1 promoter. *Journal of virology* 79: 5880-
885 5885
886 Yue W, Shackelford J, Pagano JS (2006) cdc2/cyclin B1-dependent phosphorylation of EBNA2
887 at Ser243 regulates its function in mitosis. *Journal of virology* 80: 2045-2050
888 Yun S-M, Moulaei T, Lim D, Bang JK, Park J-E, Shenoy SR, Liu F, Kang YH, Liao C, Soung N-
889 K *et al* (2009) Structural and functional analyses of minimal phosphopeptides targeting the polo-
890 box domain of polo-like kinase 1. *Nature structural & molecular biology* 16: 876-882
891 Zdimerova H, Murer A, Engelmann C, Raykova A, Deng Y, Gujer C, Rühl J, McHugh D, Caduff
892 N, Naghavian R *et al* (2020) Attenuated immune control of Epstein-Barr virus in humanized
893 mice is associated with the multiple sclerosis risk factor HLA-DR15. *European journal of*
894 *immunology*
895

896 **FIGURE LEGENDS AND TABLES**

897 **Figure 1**

898 **EBNA2 and PLK1 complexes in EBV infected B cell lines**

899 Co-immunoprecipitation (IP) of EBNA2 (A) and PLK1 (B) using EBNA2-, PLK1-specific
900 antibodies, or isotype-matched control antibodies performed on total cell lysates (L) of EBV
901 immortalized B cells.

902

903 **Figure 2**

904 **EBNA2/PLK1 phosphorylation-dependent complex formation**

905 Transfection and immunoprecipitation of (A) HA-tagged or for smaller fragments (B) GFP-
906 tagged EBNA2 fragments to co-precipitate endogenous PLK1. Total protein lysates and
907 immunoprecipitates (IP) were analyzed by Western blotting (WB). (C) Schematic outline of
908 EBNA2, its dimerization domains (END, DIM), the region used by CBF1 to recruit EBNA2 to
909 DNA (WW), the C-terminal transactivation domain (TAD), the nuclear localization signal (N) and
910 the EBNA2 fragments used to map the PLK1 docking site (UniProt ID: P12978.1). The panel on
911 the right summarizes the results of the co-immunoprecipitations in (A) and (B). (D) Multiple

912 sequence alignment (left) and superposition (right) of several phosphopeptides present in
913 published crystal structures of PLK1 PBD (phosphorylated residues stained red). Crystal
914 structures of the PBD in complex with peptides show that the positively charged groove of PBD
915 docks in a similar mode to the negatively charged phosphopeptides. References for PDB ID:
916 1Q4K (Cheng *et al*, 2003), 1UMW (Elia *et al.*, 2003a), 4E9C (Śledź *et al*, 2012), 3C5L (Yun *et*
917 *al*, 2009), 3HIK (Yun *et al.*, 2009), 5X3S (Lee *et al*, 2018), 3Q1I (Pavlovsky *et al*, 2012).
918 Potential residues of EBNA2, which might be a PBD docking site, are listed below. (E)
919 Immunoprecipitation of HA-tagged EBNA2 mutant ST266AV, TSS377VAA and SPSS467APAA
920 using HA-specific antibodies. (F) ITC thermogram of PLK1 PBD titrated with the peptide
921 PNTSSPS or the phosphopeptide PNTSpSPS of EBNA2. (G) GST-pulldown of PLK1 from total
922 cellular extracts using Cyclin B/CDK1 phosphorylated GST-EBNA2 region 342-422. (H) Co-
923 immunoprecipitation of transfected EBNA2 wt or S379A and endogenous PLK1.

924

925 **Figure 3**

926 **PLK1 phosphorylates the EBNA2 residue S457 and T465 within the C-terminal transactivation** 927 **domain**

928 (A) Doxycycline (Dox) induction of EBNA2 in DG75^{Dox HA-EBNA2} cells treated for 24 hours. Co-
929 immunoprecipitates of HA-EBNA2 and endogenous PLK1 are visualized by Western blotting.
930 (B) EBNA2/PLK1 co-precipitates were submitted to kinase reactions using [γ -³²P] ATP in the
931 absence (control) or presence of 50 ng recombinant active PLK1. (C) EBNA2 co-precipitates
932 were submitted to kinase reactions in the absence (control) or the presence of the PLK1
933 inhibitor Volasertib (40 nM). (D) EBNA2 candidate phosphorylation mutants were expressed in
934 DG75 B cells and tested for PLK1 binding by co-immunoprecipitations followed by Western
935 blotting. (E) Immunoprecipitates were submitted to kinase reactions as in B, but samples were
936 treated with Volasertib (40 nM) (+) or treated with solvent only (-). (F) GST EBNA2 fragment
937 246-487 wt and mutant S457A/T465V were treated with recombinant active PLK1 (+) in the
938 presence of [γ -³²P] ATP in vitro or left untreated (-). CRS, an artificial PLK1 test substrate (Yuan
939 *et al*, 2002), was used as a positive control. (G) Schematic presentation of EBNA2
940 phosphorylation sites by CDK1 and PLK1. (H) HA-tagged EBNA2 candidate phosphorylation
941 mutants were expressed in DG75 B cells and tested for activation of an EBNA2/CBF1
942 responsive promoter reporter luciferase plasmid. Activation of the reporter gene is shown as
943 relative response ratio normalized to Renilla luciferase activity and shown relative to wt activity.
944 (I) GST-pull down assay using GST-EBNA2 446-474 as a bait to purify cellular proteins from

945 DG75 cells followed by Western blotting and quantification of signals obtained by GST and p300
946 specific antibodies. Relative binding affinities (rel. p300 bindg.) are normalized to the wt signal.

947

948 **Figure 4**

949 **PLK1 inhibits EBNA2 activity by phosphorylating residues S457/T465**

950 (A) Flag-tagged active (PLK1) and kinase inactive PLK1 (K82M) were co-expressed with HA-
951 EBNA2 wt, docking site mutant (S379A) and phosphorylation mutant (S457A/T465V) and tested
952 for activation of an EBNA2/CBF1 responsive promoter reporter. Activation of the reporter firefly
953 luciferase gene is shown as relative response ratio normalized to Renilla luciferase activity and
954 shown relative to EBNA2 wt activity. (B) 30 µg of cellular extracts that were produced for
955 luciferase assays were tested for protein expression using Flag-, HA and GAPDH specific
956 antibodies.

957

958 **Figure 5**

959 **EBV strains expressing EBNA2 mutants deficient for PLK1 docking or phosphorylation accelerate 960 B cell proliferation and express elevated levels of the viral LMP1 protein.**

961 (A) Primary B cells were stained with cell trace violet before they were infected and cell cultures
962 were started. Loss of the fluorescent cell tracking dye was recorded by flow cytometry to
963 monitor proliferation on day 0, 4 and 6 post-infection. Mean values for 3 biological replicates,
964 standard deviation and significance of changes in signal loss of mutants compared to wild-type
965 controls (p-value, *: $p < 0.05$; ****: $p < 0.0001$). (B) Long-term growth transformed B cell cultures
966 infected with recombinant EBV mutants were seeded at a starting concentration of 2×10^5 cells
967 per ml. Data were presented as the mean \pm S.E.M. of $n = 4$ biological replicates. Statistical
968 significance was tested by two-way ANOVA followed by a Tukey's multiple comparison test (*: P
969 < 0.05 , **: $P < 0.01$, ****: $P < 0.0001$, vs WT).

970 (C) Expression of EBNA2, LMP1, PLK1, MYC, and GAPDH was analyzed by Western blotting
971 and immunostaining of whole cell extracts of cell lines established from 3 individual donors.

972

973 **Figure 6**

974 **EBV strains carrying EBNA2 mutants with diminished PLK1 binding or resistant to PLK1 975 phosphorylation cause lymphomas in humanized mice more frequently than EBV wt.**

976 (A) Experimental set-up. (Images of animals, syringes and blood collection tubes are derived
977 from Servier Medical Art.) (B) Survival curve of humanized mice infected with 10^5 GRU EBV wt
978 ($n = 13$), EBV S379A ($n = 11$) or EBV S457A/T465V EBV ($n = 9$). Log-rank test. (C) Percentage

979 of mice having macroscopically visible tumors at the day of sacrifice. Numbers within bars
980 indicate the total number of mice with or without tumors in the respective groups. Fisher's Exact
981 test. (D) Viral loads in spleen of infected humanized mice at the day of sacrifice. Error bars
982 indicate mean \pm SEM. EBNA2 WT EBV: n = 13; EBNA2 S379A EBV: n = 11; EBNA2 S457A
983 T465V EBV: n = 9. (E) Development of viral loads in blood of infected mice over a period of five
984 weeks. Error bars indicate mean \pm SEM. Mann-Whitney U test. (F) Flow-cytometric analyses of
985 CD8⁺/CD4⁺ T cell ratios in the blood of infected mice over a period of five weeks. Error bars
986 indicate mean \pm SD.
987

988

989 **Table 1**

990 **IgH V gene analysis of B cell lymphoproliferations**

Mouse	Tissue	EBV	Clonality	VH subgroup or gene ^a	DH gene ^{b,c}	JH gene ^c	Reading frame ^c
#13	spleen	wt	poly poly poly	VH1 VH3 VH4			
#23	spleen	S379A	poly poly poly	VH1 VH3 VH4			
#23	peritoneum	S379A	mono	VH3-15	DH3-10	JH4	in-frame
#15	spleen	S379A	mono mono	VH2-70 VH1-45	DH3-16 DH6-13	JH4 JH4	in-frame out-of-frame
#15	peritoneum	S379A	mono mono	VH4-39 VH1-2	DH6-6 n.i.	JH4 JH4	out-of-frame in-frame
#8	lymph node	S457A/T465V	poly mono	VH1 VH4-39	n.i.	JH4	in-frame
#18 ^d	spleen	S457A/T465V	mono poly oligo/poly mono	VH3-30 VH1 VH3 VH1-2	DH6-19 DH2-15	JH6 JH4	in-frame out-of-frame

991

992 ^aIf only the VH subgroup is specified, this means that PCR products were obtained for these subgroups
 993 (typically for the three largest subgroups VH1, VH3, and VH4), and that a polyclonal composition was
 994 revealed upon direct sequencing of these amplicates.

995 ^bn.i.: D gene sequence was not identified

996 ^cSanger sequencing results obtained from monoclonal tumor specimen

997 ^dSpecimen were taken from different parts of the spleen

998

999

1000

1001 **Table EV1**

1002 **19 candidate EBNA2 associated proteins identified by label free mass spectrometry**

1003

1004

1005

ensemble-ID	Peptide count ^a	Peptides used for quantification ^b	Confidence score ^c	Anova (p)	Accumulation ^d	Symbol	Replicate 1 ^e vector (empty)	Replicate 2 ^e vector (empty)	Replicate 3 ^e vector (empty)	Replicate 1 ^e EBNA2 wt	Replicate 2 ^e EBNA2 wt	Replicate 3 ^e EBNA2 wt	Description
ENSP00000248958	1	1	48	0.00	1652	SDF2L1	27	0	0	4799	33098	6503	stromal cell-derived factor 2-like 1
ENSP00000247020 E	2	2	54	0.01	762	SDF2	26	0	0	2392	14742	2515	stromal cell-derived factor 2
ENSP00000342070	2	2	85	0.04	177	CTSB	56	0	36	11264	330	4616	cathepsin B
ENSP00000380376	1	1	34	0.01	164	PAXIP1	13	27	2	338	4697	1748	PAX interacting (with transcription-activation domain) protein 1
ENSP00000311766	13	1	336	0.04	125	ATAD3B	59	37	0	469	9408	2205	ATPase family, AAA domain containing 3B
ENSP00000300093	7	7	172	0.01	77	PLK1	1610	407	198	14583	122709	32353	polo-like kinase 1
ENSP00000265028	5	5	207	0.01	46	DNAJB11	1645	2063	2421	20887	211659	49942	DnaJ (Hsp40) homolog, subfamily B, member 11
P12978.1	5	5	162	0.01	26	EBNA2	5841	3949	3629	41868	251544	59586	Epstein-Barr nuclear antigen 2
ENSP00000305815	1	1	26	0.01	26	CBF1/RBPJ	410	121	93	1602	10431	4182	recombination signal binding protein for immunoglobulin kappa J region
ENSP00000261893	7	7	210	0.01	17	LACTB	5688	3130	2773	21048	129818	47963	lactamase, beta
ENSP00000368030	18	6	544	0.03	11	ATAD3A	13872	9774	4851	41200	213392	45267	ATPase family, AAA domain containing 3A
ENSP00000446596	3	2	105	0.05	10	DYNLL1	13993	9084	6329	25470	217534	46037	dynein, light chain, LC8-type 1
ENSP00000277900	5	4	100	0.05	7	ADD3	6551	765	819	12200	35354	9851	adducin 3 (gamma)
ENSP00000306223	2	2	32	0.03	4	SNRPN	508	154	254	1595	1306	639	small nuclear ribonucleoprotein polypeptide N
ENSP00000280326	2	2	47	0.05	2	CCT5	950	950	1819	1867	3216	4077	chaperonin containing TCP1, subunit 5 (epsilon)
ENSP00000295688	2	2	45	0.03	2	CCT3	1269	1133	1066	1579	1979	2715	chaperonin containing TCP1, subunit 3 (gamma)
ENSP00000261182	1	1	35	0.01	2	NAP1L1	1081	843	707	1562	1580	1540	nucleosome assembly protein 1-like 1
ENSP00000272163	1	1	29	0.01	2	LBR	1550	1597	1653	2133	3232	2798	lamin B receptor
ENSP00000238081	4	3	123	0.00	2	YWHAQ	5744	5869	7103	9673	10151	10026	tyrosine 3-monooxygenase/tryptophan 5-monooxygenase activation protein, theta polypeptide

1006

1007 **Table EV1 Footnotes**

1008 ^a Number of peptides detected during mass spectrometric analysis.

1009 ^b only peptides specific for the protein were used for quantification.

1010 ^c The confidence score reflects the combined scores of all observed mass spectra that can be matched to amino acid
1011 sequences within that protein. A higher score indicates a more confident match.

1012 ^d This value reflects the accumulation of proteins found after immunoprecipitation using EBNA2 wt as a bait
1013 compared to the proteins found using no bait (empty vector). The value was calculated by dividing the mean values of
1014 the normalized abundances (see footnote ^e).

1015 ^e Normalized abundances derived from mass spectrometric analysis.

1016

1017 **Figure EV1**

1018 **Annotated HCD MS/MS spectra of phosphopeptides**

1019 (A) LVQPHVPLRPTAPTILSPLSQPR, (B) MHLPLVHVPDQSMHPLTHQSTPNPDSPEPR, (C)
1020 DLDESWDYIFETTESPSSDER, (D) TTESPSSDEDYVEGPSKRPRPSIQ, and (E)
1021 DYVEGPSKRPRPSIQ, bearing 5 confidentially localized phosphorylation sites, S184, 258, 457,
1022 T465, and S479, respectively. The “ph” denotes phosphosites localized. The a-, b-, and y- ions
1023 are in pale blue, dark blue, and red, respectively. Ions with neutral losses are in orange, internal
1024 fragment ions in purple, ammonium ion in green, and side-chain loss in turquoise. The asterisk
1025 (*) denotes loss of H₃O₄P with a delta mass of 97.9768 from the phosphorylated fragment ion.

1026

1027 **Figure EV2**

1028 **Overview of sequence coverage and phosphorylation sites identified by mass**
1029 **spectrometry**

1030 (A) 6x His-tagged EBNA2 (A) and (B) GST-EBNA2 453-474 phosphorylated by PLK1. Proteins
1031 were expressed in E. coli and extracted after SDS-PAGE separation, digested by trypsin (green
1032 bars) and V8 (blue bars) in parallel and submitted to LC-MS/MS (enlarged letters in red or
1033 green). The sign # denotes Arg (R) inserted to facilitate fragmentation. The asterisk (*) denotes
1034 the initial Met (M) of EBNA2. Proteins before phosphorylation by PLK1 were studied in parallel
1035 but no phosphorylation sites were identified. The sequence corresponds to UniProt ID:
1036 P12978.1.

1037

1038 **Figure EV3**

1039 **Construction of EBV BACmids carrying HA-tagged EBNA2 mutants impaired for PLK1 binding or**
1040 **PLK1 phosphorylation and functional tests in cell culture.**

1041 (A) Electrophoretic separation of the restriction digest of EBV Bac DNA: p6008 (precursor),
1042 pXZ135 (insertion of Kan/rpsL as a precursor for EBV HA-EBNA2) and pXZ143 (EBV HA-
1043 EBNA2=EBV wt). The arrows highlight distinct fragments that characterize the individual BACs
1044 in size upon Kan/rpsL insertion and deletion (6005 bp → 7353 bp → 6035 bp). Molecular
1045 markers: λ DNA-Hind III digest (nonitalics) and λ DNA-BstE II digest (italics). (#) denotes the
1046 fragment derived from fragments denoted by asterisks (*). (B) Sanger sequencing of pXZ143 to
1047 confirm the insertion of the HA-tag into EBNA2 in the backbone of p6008 (C, D) Sanger
1048 sequencing of pXZ203 (C) and pXZ146 (D) to confirm the substitution of S379A and
1049 S457A/T465V, respectively. (E) Gating strategy of cell trace violet stained active B cells after
1050 EBV infection. (F) Adenoid B cells were stained with cell trace violet before they were infected
1051 with EBV mutants as indicated and analyzed by flow cytometry.

1052

1053 **Figure EV4**

1054 **T cell subpopulations of blood and spleen of infected mice**

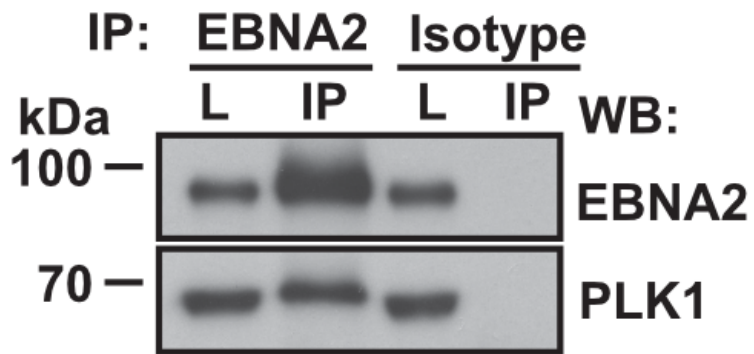
1055 Flow-cytometric analyses of (A) CD8⁺ or (B) CD4⁺ T cell percentages and (C) CD8⁺ and (D)
1056 CD4⁺ T cell activation in the blood of mice infected with wt or mutant EBV over a period of five
1057 weeks. (E) Percentages of CD4⁺ and CD8⁺ subpopulations and activation of (F) CD4⁺ and (G)
1058 CD8⁺ subpopulations. Analyses of the spleens for (H) CD8⁺ and (I) CD4⁺ naïve, terminally
1059 differentiated (Temra), central memory (TCM) and effector memory (Tem) memory T cell
1060 subpopulations. (The shape of data points indicates to which cohort (experiment 1, 2 or 3) the
1061 respective animal belongs while the color indicates the EBV strain. Statistical significance was
1062 tested using the Mann-Whitney U Test with Holm-Sidak correction for multiple comparisons.

1063

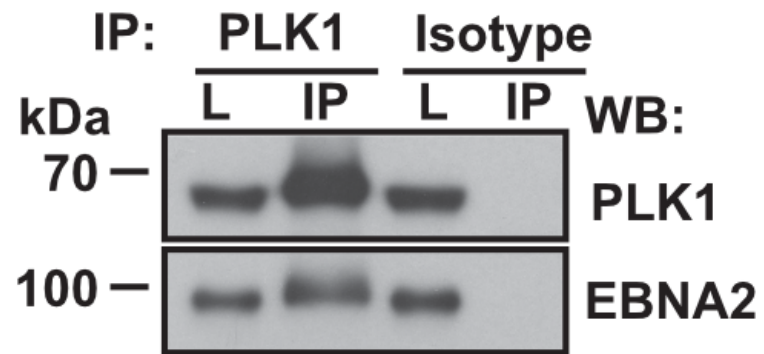
1064 **APPENDIX**

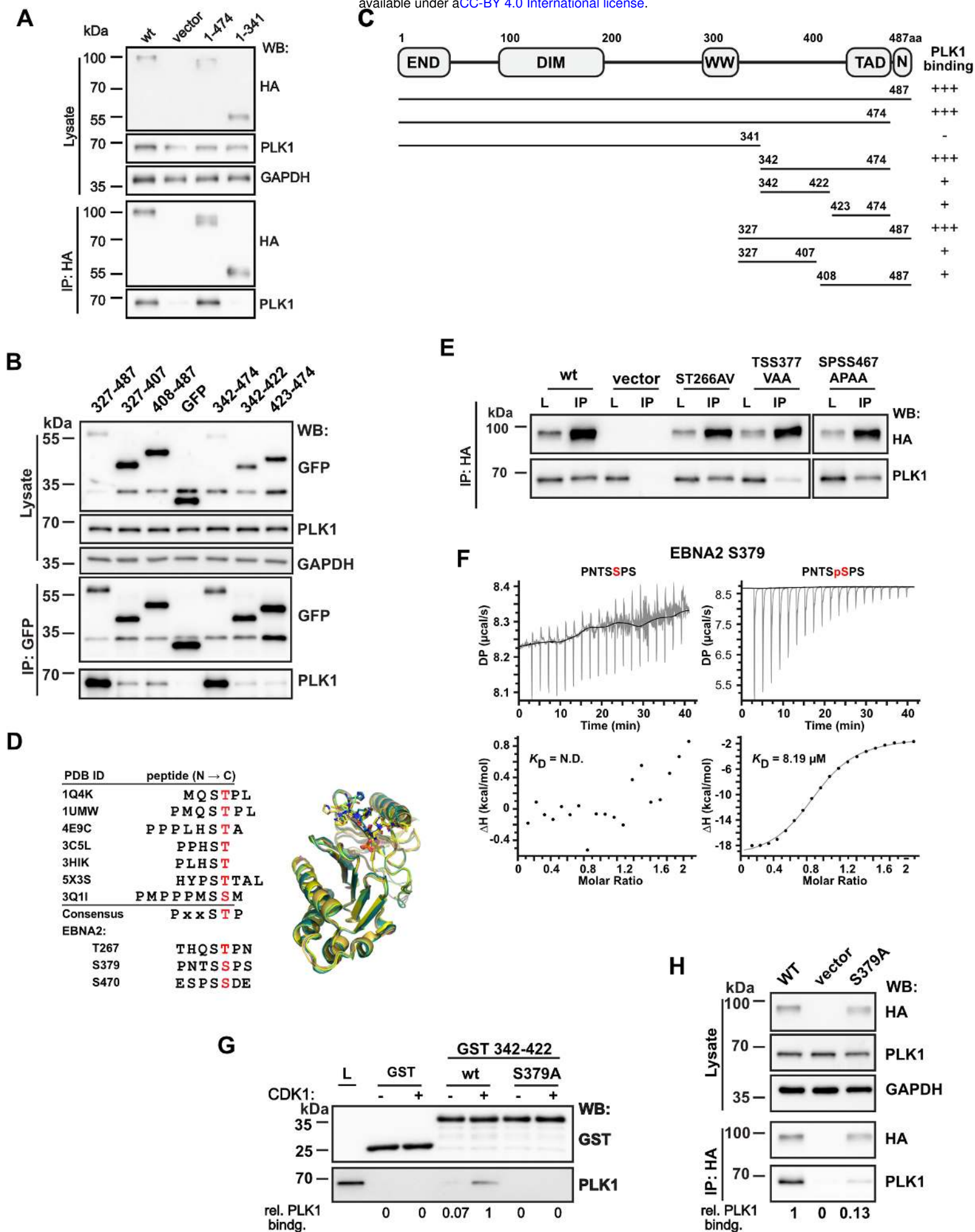
1065 Supplementary Table S1 (List of oligonucleotides used in this study)

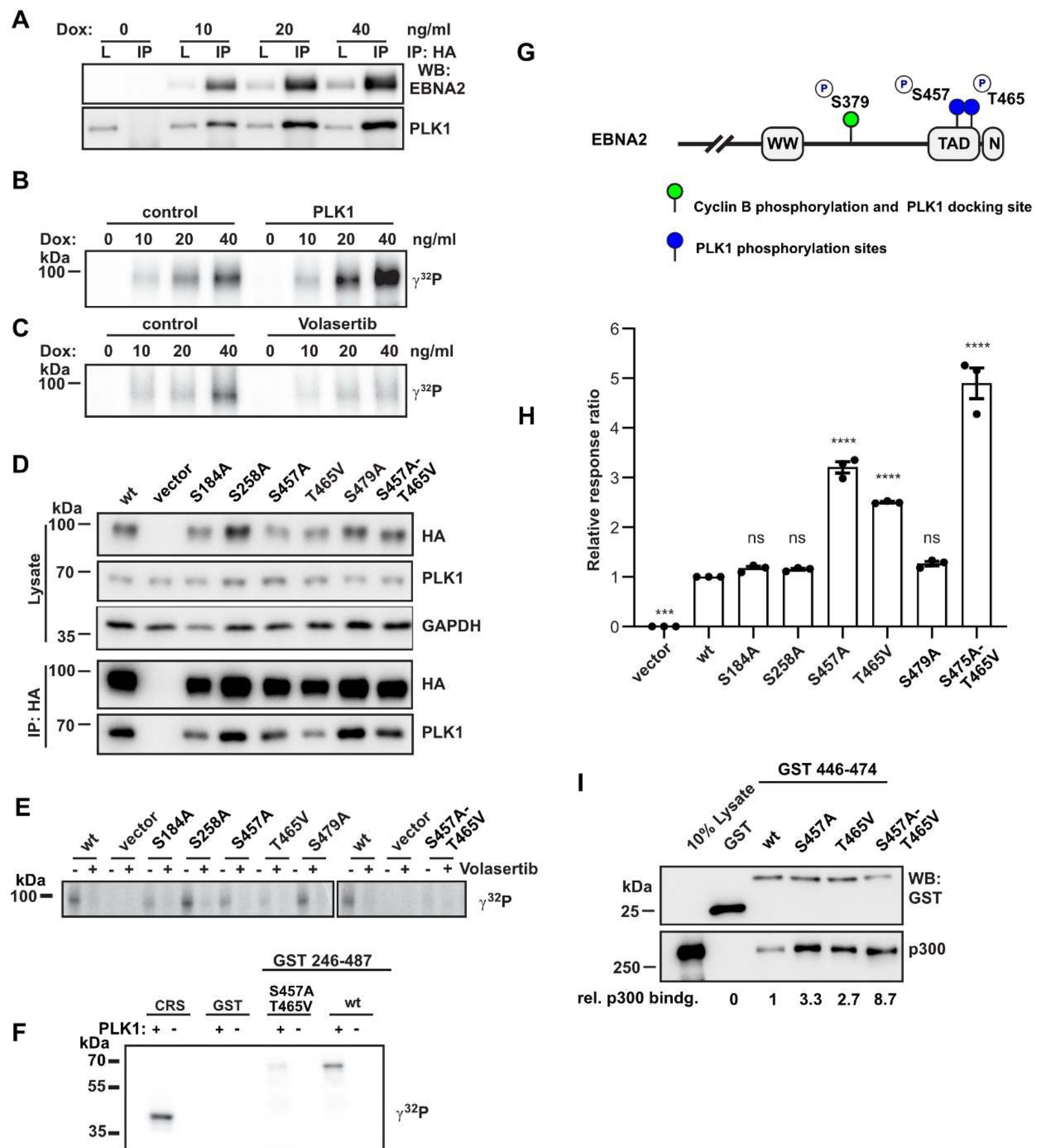
A



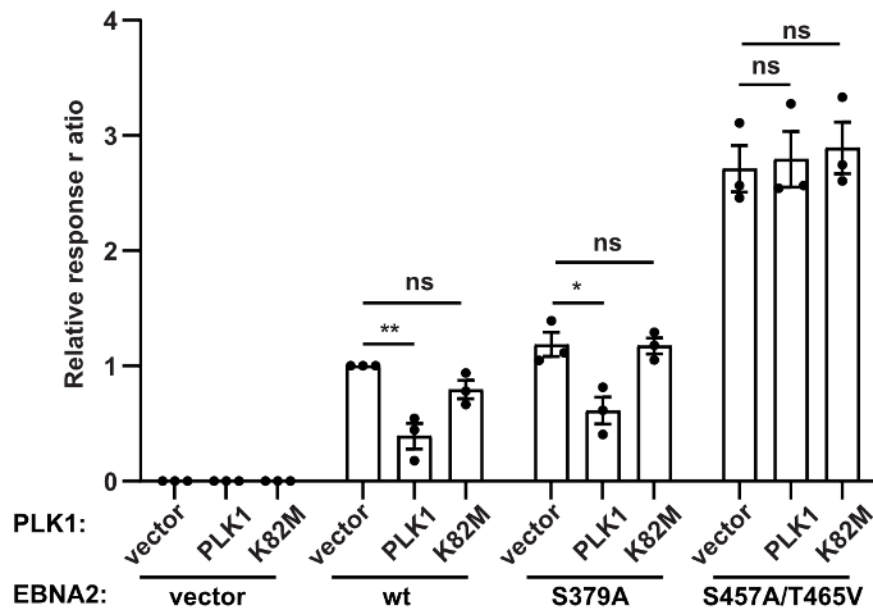
B



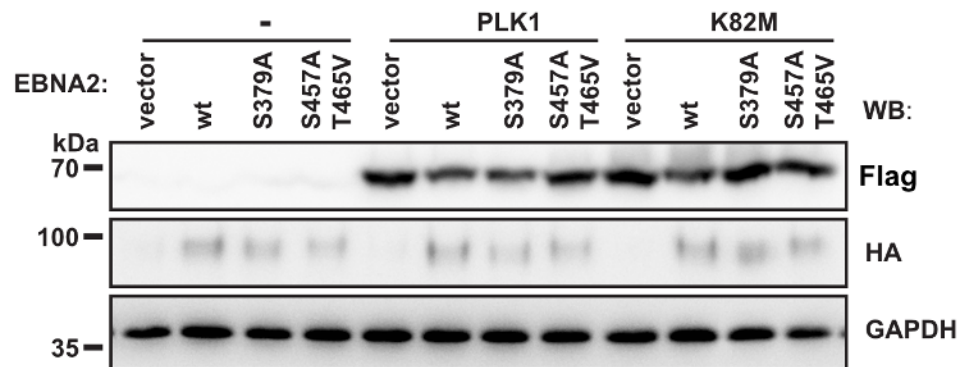


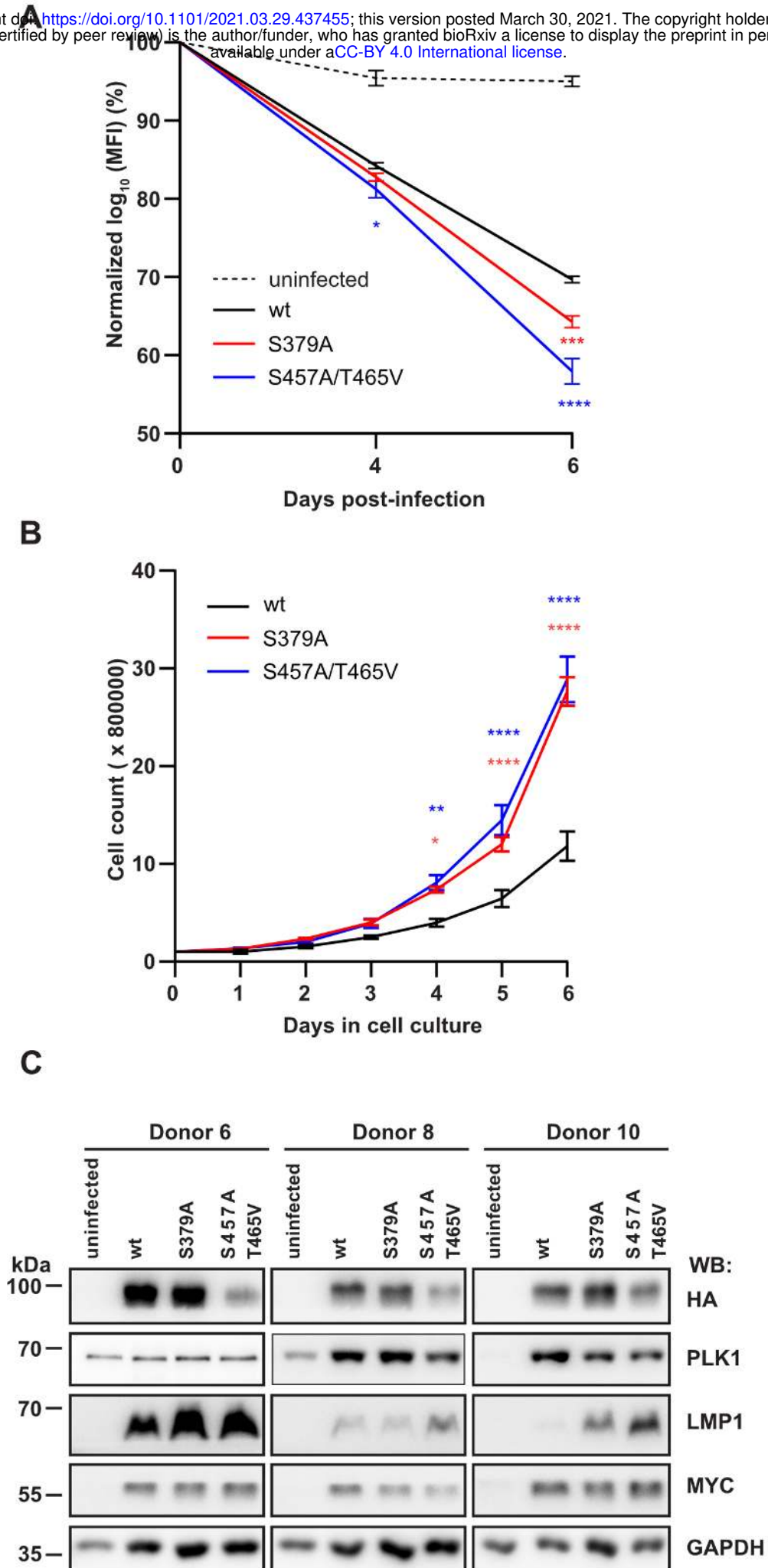


A



B

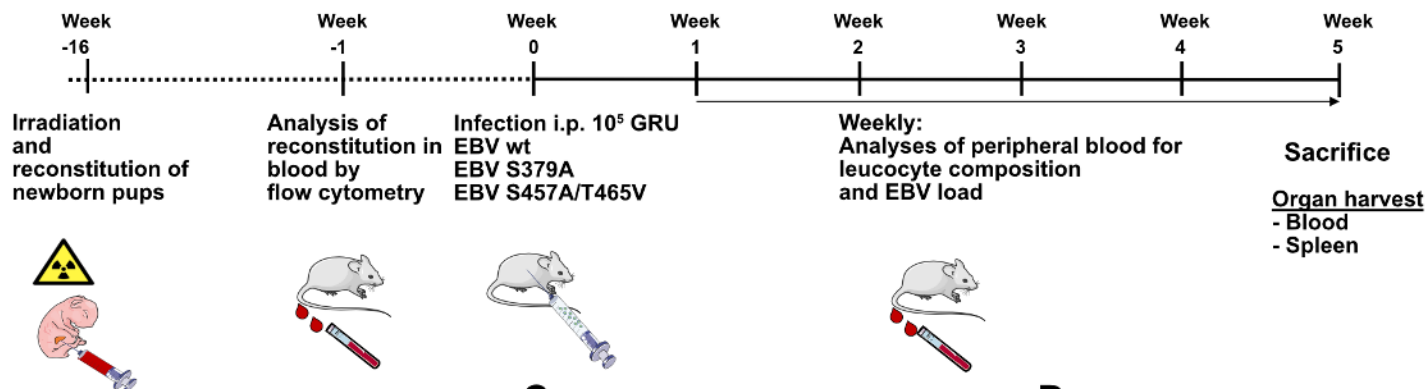




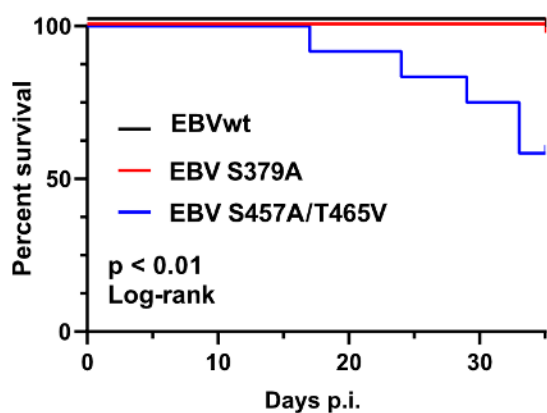
Generation of huNSG mice

Analyses of infected huNSG mice

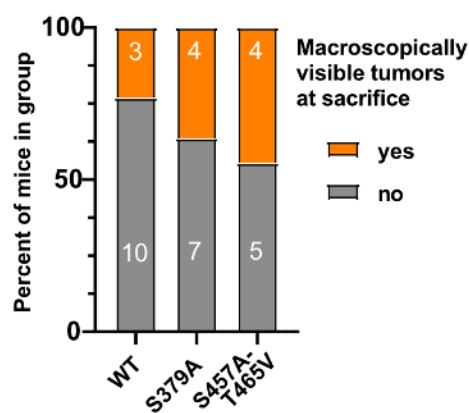
A



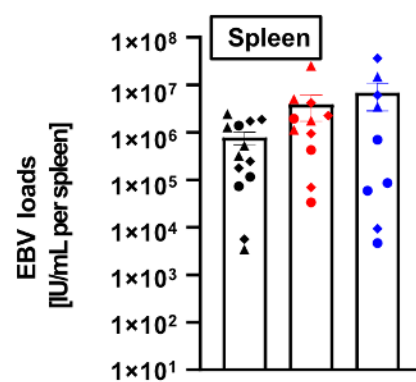
B



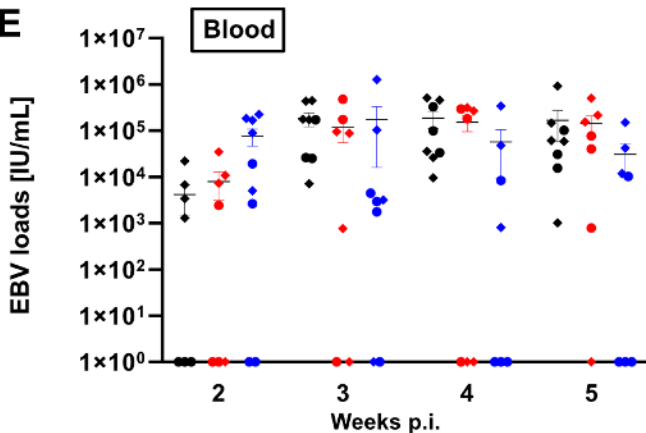
C



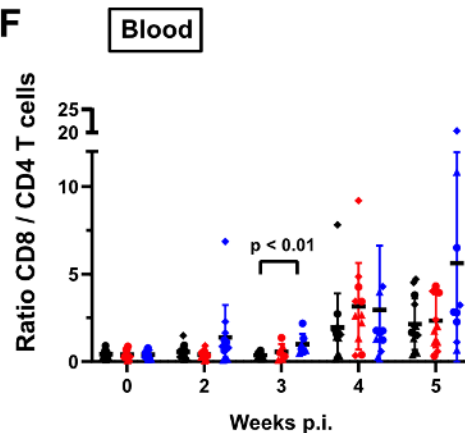
D



E



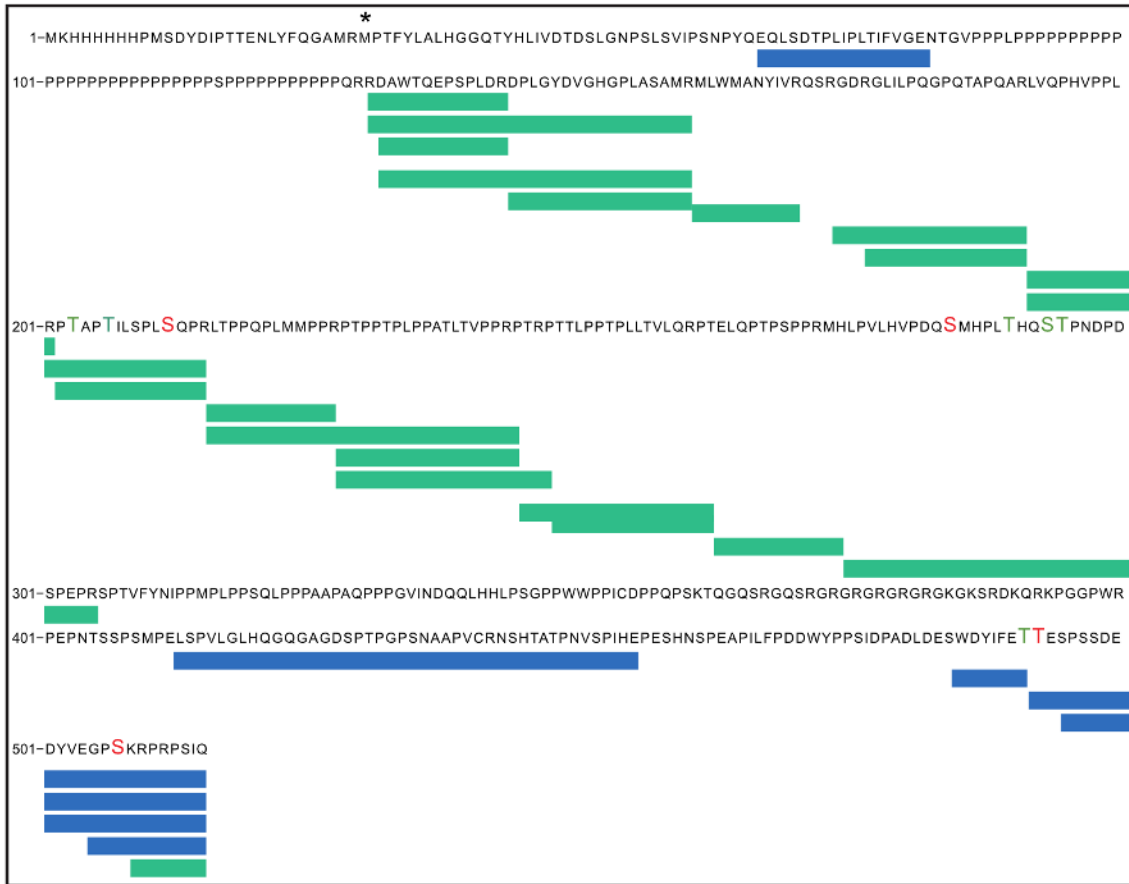
F



experiment	1	2	3
wt	● ▲ ◆		
S379A	● ▲ ◆		
S457A/T465V	● ▲ ◆		

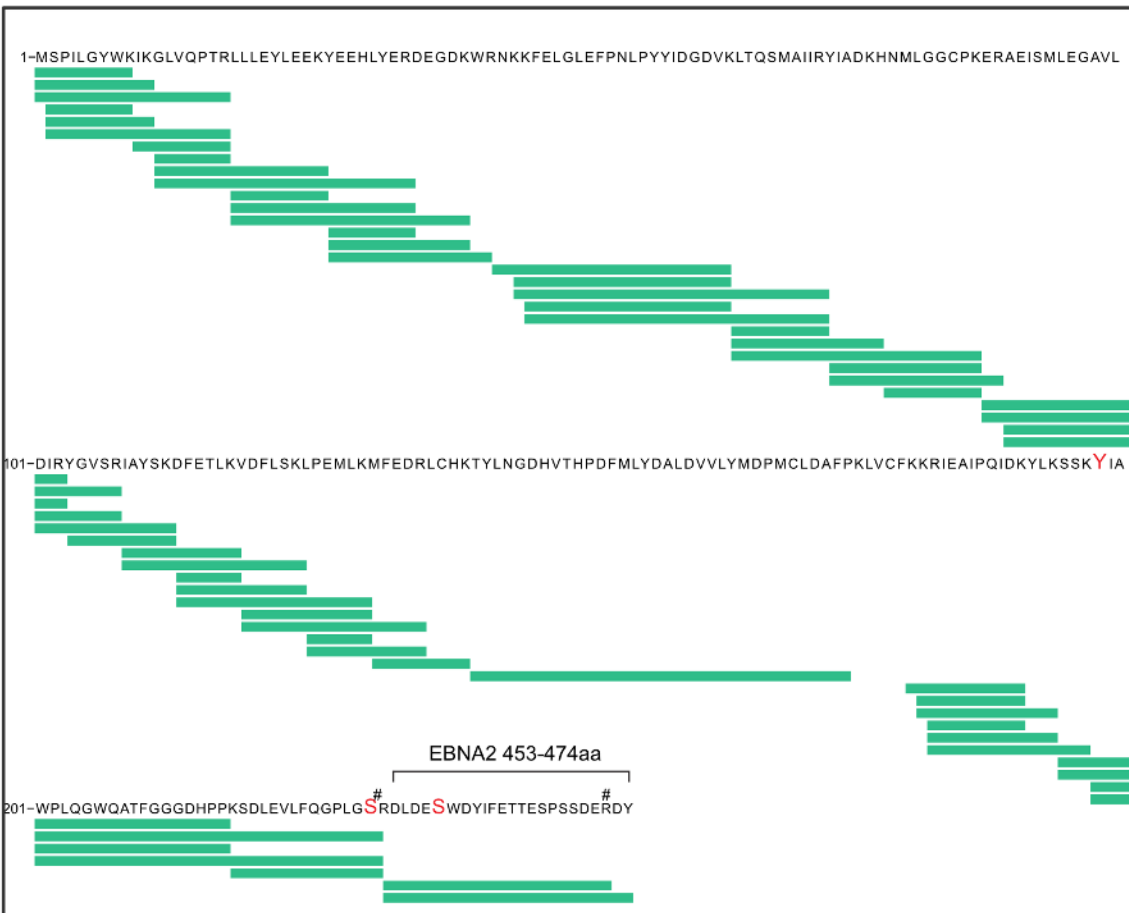
HIS(6x)EBNA2 1-487

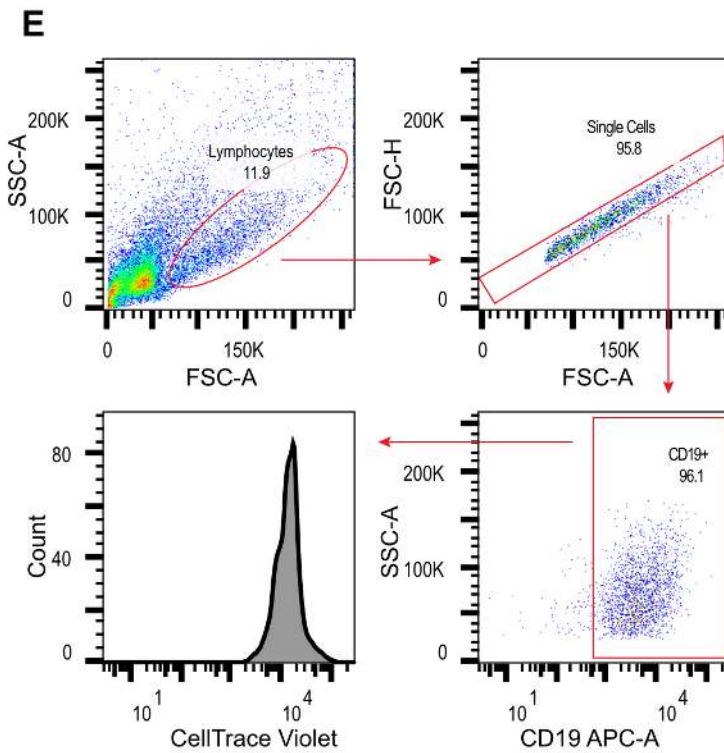
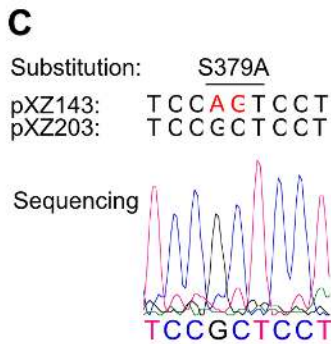
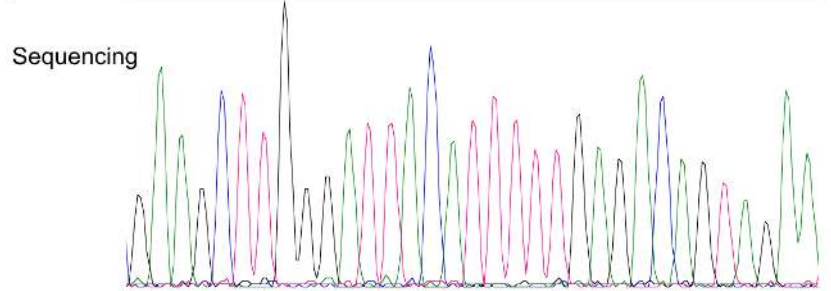
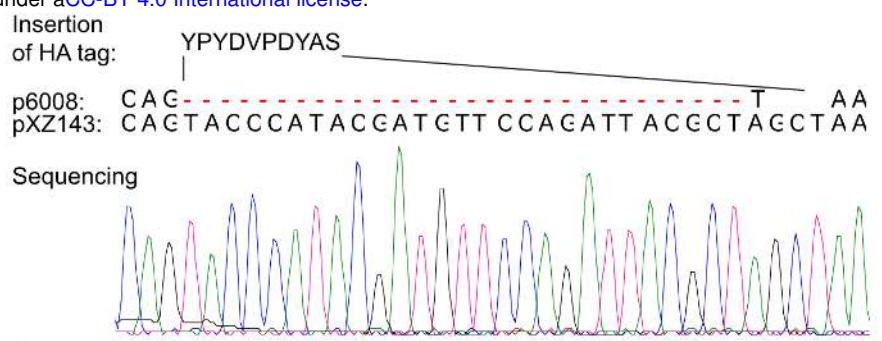
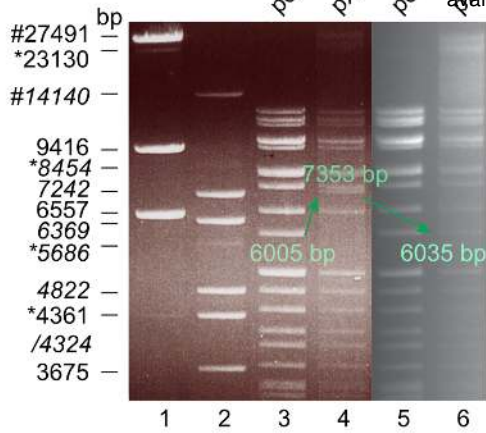
A



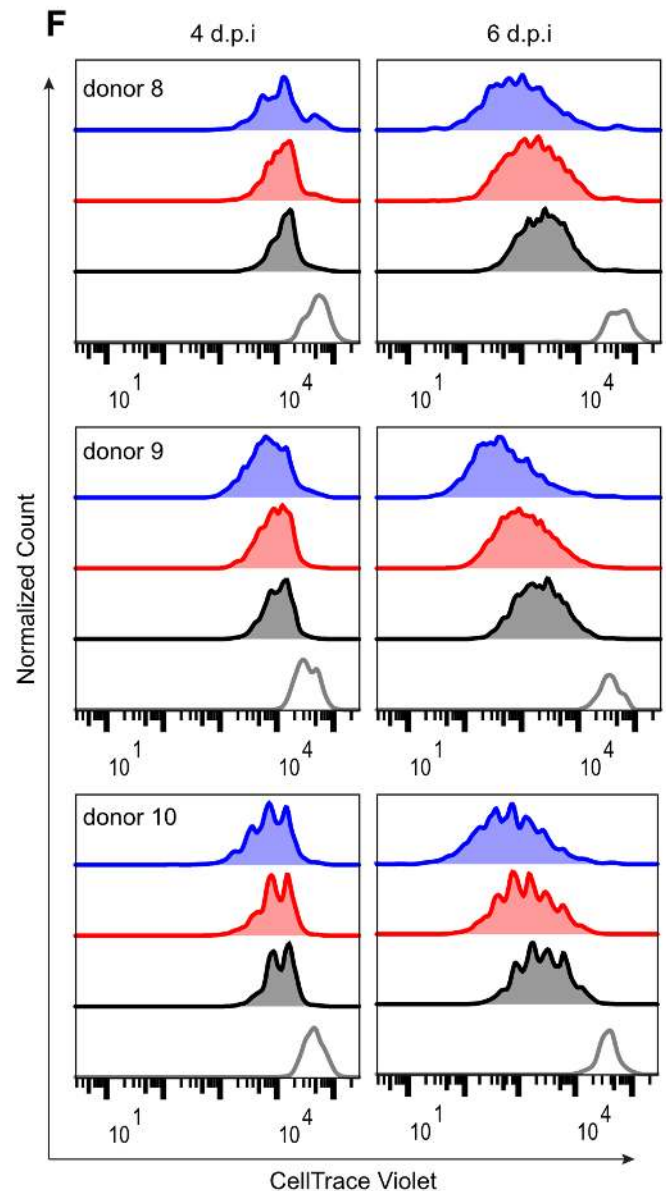
GST-EBNA2 453-474

B



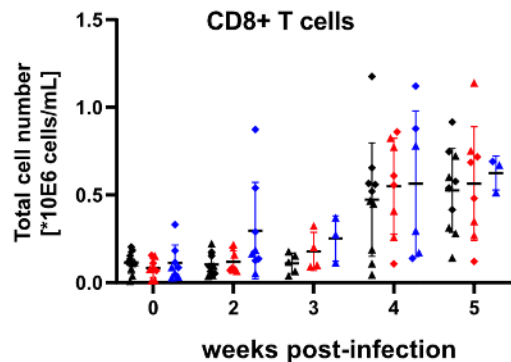


■ S457A/T465V
■ S379A
■ wt
■ uninfected

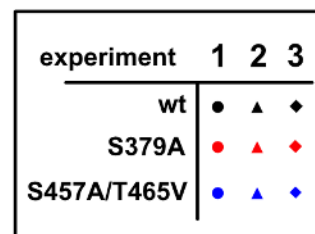
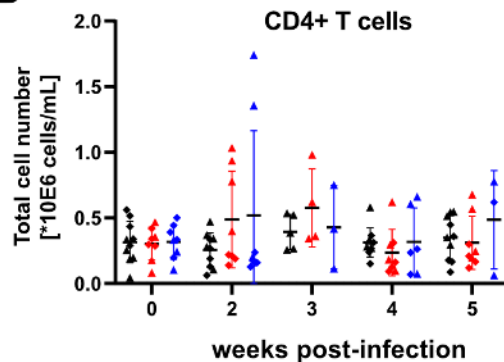


BLOOD

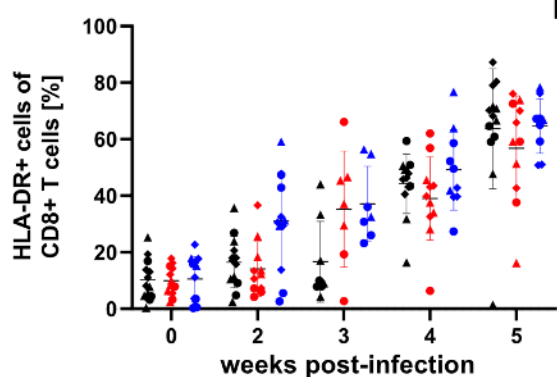
A



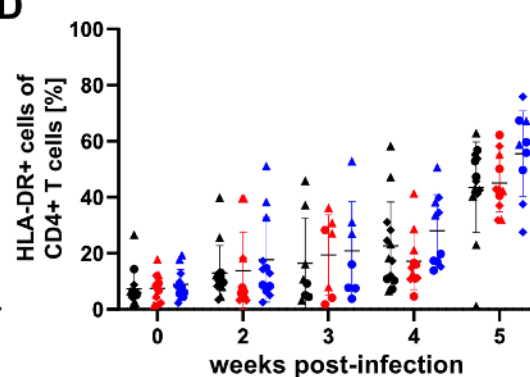
B



C

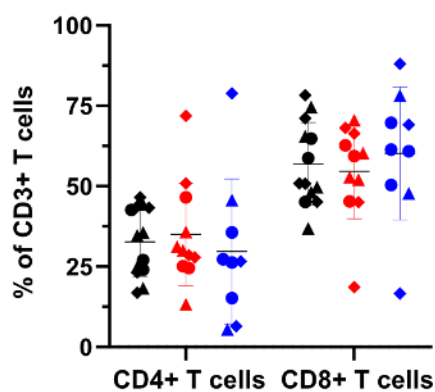


D

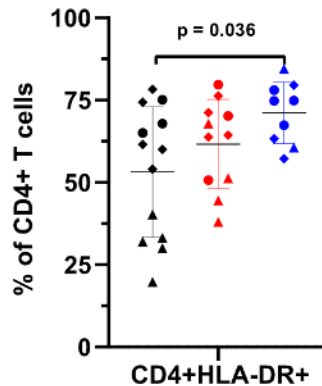


SPLEEN

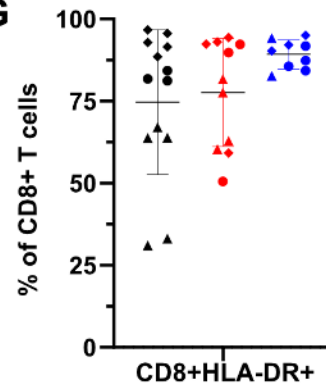
E



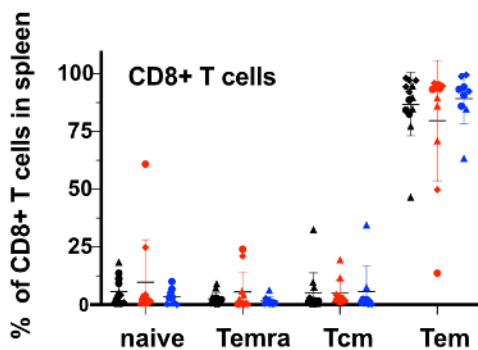
F



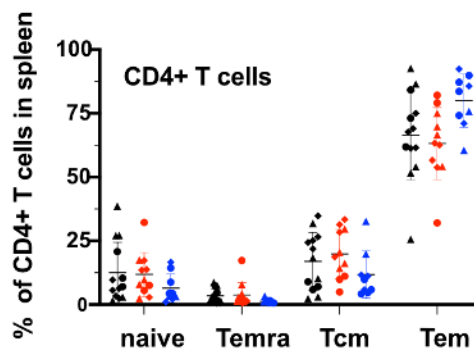
G



H



I



Spleen:

EBV wt (N=13)

EBV S379A (N=11)

EBV S457A/T465V (N=9)